CORRECTIONS FOR NEAR SURFACE EFFECTS: DECOMPOSITION OF THE MAGNETOTELLURIC IMPEDANCE TENSOR AND SCALING CORRECTIONS FOR REGIONAL RESISTIVITIES: A TUTORIAL

ROSS W. GROOM[1] and KARSTEN BAHR[2]

[1]*Geological Survey of Canada, Ottawa, Canada*
[2]*Institut fur Meteorologie und Geophysik, Frankfurt am Main, Germany*

(Received 27 June 1991; accepted 30 October 1991)

Abstract. This paper primarily examines the effects of small-scale or near-surface conductivity inhomogeneities on the magnetotelluric (MT) impedance tensor. These effects cause three different types of distortion results. (1) The well-known *static shifts* of sounding curves. (2) When the underlying regional setting is two-dimensional then the two regional impedances are mixed in an arbitrary coordinate system. Thus the level and shape of each sounding curve is distorted as are the phases. (3) At sufficiently high frequencies these effects generate anomalous magnetic fields that in turn alter the background phases.

This tutorial first explores the usefulness of various MT tensor analysis techniques to overcome the problem of phase mixing and to recover regional information in the presence of local geological noise. Synthetic and experimental data are considered. A sequence of *a priori* models of increasing complexity are described. The use of appropriate decompositions of the MT tensor each with an increasing number of parameters is emphasised. In a second part, phase mixing and static shifts are examined from a synoptic view. Some static shift removal techniques that can be used in conjunction with the decomposition are discussed. This paper is not a review but rather an investigation of a few methods that the authors have found useful with field data.

Introduction

Two useful *a priori* models for the magnetotelluric impedance tensor have existed for some time. The first, introduced by Cagniard (1953), is a model for 1D structures in which there are 2 related parameters at each frequency (phase and impedance magnitude). These 2 parameters are expected to vary smoothly with frequency. The second model, introduced for practical applications essentially by Swift (1967), extends the parametrization to 2D structures. In this factorization, there are up to 5 parameters per frequency. The strike parameter is expected to be relatively constant with frequency while the 2 complex impedances should vary smoothly with frequency. However experimentally determined impedance tensors often do not conform to either of these ideal models.

Rarely can the conducting structures which are significant in producing the measured electromagnetic fields in the earth, be approximated as one or two dimensional over the entire frequency range of interest to the investigator. However, in many cases the geological features of principal interest do have a dimensionality less than three over some subset of the frequency band. Too often in

Surveys in Geophysics **13**: 341–379, 1992.

these cases, the measured fields are significantly contaminated by 3D scattering effects of relatively small structures which are either of little interest to the investigator or too spatially undersampled to allow interpretation. If these structures are small then necessarily they must be near the surface to produce distinct scattered fields rather than merely contributing to an effective bulk response. Techniques for the understanding and removal or suppression of these small-scale, yet significant, scattering effects are the subject of the tutorial.

As a tutorial, the purpose of this paper is not to review the literature with regard to the effects of 3D scattering in magnetotellurics but rather to summarize the authors' experiences with specific techniques for dealing with such local scattering effects. Excellent reviews are already present in Jones (1983), Jiracek (1990) and Cerv and Pek (1990). In this tutorial, there is a strong emphasis on the use of decomposition techniques in magnetotellurics; some methods which can be used in conjunction with such techniques; and the relationships between specific decomposition methods and other techniques. The subject is examined from three-points of view: (1) theoretical justification of concepts, (2) examples using synthetic data and (3) examples with experimental data.

Small-Scale 3D Electromagnetic Scattering

Although any 3D anomaly will have a galvanic response (mainly due to charges on boundaries) which interacts with an inductive response (due to internal vortex-like currents), the significance of the inductive contribution over the galvanic contribution is expected to decay with increasing period (West and Edwards, 1985). If the scattered or secondary fields are due to isolated and confined anomalous conductivity structures, then the inductive response will eventually become weak as frequency decreases but charges on conductivity gradients can still strongly distort the measured horizontal electric field, $\vec{E}$. In this case, the measured electric field is often assumed to be approximately related to the background (regional) surface electric field, $\vec{E}_0$, through a real distortion matrix $\mathbf{C}$. Thus (Bahr, 1988),

$$\vec{E}(\vec{r}) = \mathbf{C}(\vec{r})\vec{E}_0(\vec{r}) = \begin{pmatrix} C_{xx}(\vec{r}) & C_{xy}(\vec{r}) \\ C_{yx}(\vec{r}) & C_{yy}(\vec{r}) \end{pmatrix} \vec{E}_0(\vec{r}). \tag{1}$$

Equation (1) is only appropriate for a subset of all 3D scattering situations but the use of this equation in magnetotellurics has never been rigorously justified from a theoretical perspective.

We will show that several conditions must hold for Equation (1) to be strictly correct. Probably the most important of these conditions is that the spatial gradients of the background field be small over the scale size of the 3D inhomogeneity. In other words, the background field should be essentially constant over the 3D

scattering body. This obviously requires the body to be small compared to the wave length or skin depth in the host. In addition, it must be sufficiently removed from any other conductivity boundaries that the spatial gradients of scattered fields from these boundaries are minimal in the vicinity of the scatterer. That is second-order scattering must be negligible. The geometric fall-off of the scattered fields is a function of the scale size of the inhomogeneity. Therefore where there persists a significant scattered field, the local background field will be closely approximated by the background field at the scatterer due to the required small gradients. We have assumed, implicitly, that the vertical component of the surface electric field is small relative to the horizontal components which would already be imposed by the above conditions combined with the insulating nature of the atmosphere at such low frequencies.

As an example, consider a body of uniform conductivity embedded in a layered halfspace. With some assumptions, Equation (1) can be derived explicitly from the normal integral equation representation of the total electric field (e.g. Hohmann, 1976)

$$\vec{E}(\vec{r}) = \vec{E}_0(\vec{r}) + i\mu\omega \int_{V_s} g(\vec{r}, \vec{r}_s)\,\delta\sigma\vec{E}(\vec{r}_s)\,\mathrm{d}v - \\ - \frac{\nabla\nabla}{\sigma_b} \cdot \int_{V_s} g(\vec{r}, \vec{r}_s)\,\delta\sigma\vec{E}(\vec{r}_s)\,\mathrm{d}v, \tag{2a}$$

where g is the scalar Greens' function for the background and $\delta\sigma = (\sigma - \sigma_b)$ is the difference between the conductivity of the scatterer and the conductivity of the background. $\vec{E}_0$ is the background or primary electric field. $\vec{r}$ is an arbitrary measurement or field point while $\vec{r}_s$ is a source point within the scatterer. The scattered electric field in (2a) is represented by a vector (first integral) potential and a scalar potential (second expression) which are defined by integrals of the scattering currents within the body weighted by the background Greens' function.

To obtain Equation (1) from (2a), let us first assume only that the total electric field is constant over the relatively small 3D inhomogeneity. From a diffusive point of view this requires only that the scale of the scatterer be small compared to the wavelengths in the scatterer and the host. Geometrically the assumption is much more restrictive. We will see that this assumption can be much weaker. However, to illustrate we begin with the stronger assumption. Thus from (2a)

$$\vec{E}(\vec{r}) = \vec{E}_0(\vec{r}) + \left[i\mu\omega f_A(\vec{r})\vec{E}_i(\vec{r}_s) - \frac{\nabla\nabla}{\sigma_b} \cdot f_A(\vec{r})\vec{E}_i(\vec{r}_s) \right], \tag{2b}$$

where

$$f_A(\vec{r}) = \int_{V_s} \delta\sigma g(\vec{r}, \vec{r}_s)\, d\upsilon$$

and $\vec{E}_i(\vec{r}_s)$ is the total electric field at a point, $\vec{r}_s$, internal to the scatterer.

Now the total field anywhere can be described by the background field and the total field within the scatterer

$$\vec{E}(\vec{r}) = \vec{E}_0(\vec{r}) + \left[i\mu\omega f_A(\vec{r})\mathbf{I} + \frac{1}{\sigma_b}\mathbf{L}(\vec{r}) \right] \vec{E}_i(\vec{r}_s) \tag{2c}$$

where

$$\mathbf{L_{ij}}(\vec{r}) = \frac{\partial^2 f_A(\vec{r})}{\partial x_i\, \partial x_j}. \tag{2d}$$

Therefore, a simple tensor equation describes the electric fields

$$\vec{E}(\vec{r}) = \vec{E}_0(\vec{r}) + \mathbf{G}(\vec{r})\vec{E}_i(\vec{r}_s) \tag{2e}$$

for interior and exterior points where $\mathbf{G}$ is the sum of the two dyadic operators in (2c). For interior field points

$$\vec{E}_i(\vec{r}_s) = [\mathbf{I} - \mathbf{G_i}]^{-1}\vec{E}_0(\vec{r}) \tag{2f}$$

under the assumption that the background field is uniform compared to the scale of the 3D body. Since both the background and the total internal fields are assumed uniform within the scatterer, the $\mathbf{G}$ for an internal point is not a function of $\vec{r}$.

It follows that for exterior field points

$$\vec{E}(\vec{r}) = [\mathbf{I} + \mathbf{G}(\vec{r})[\mathbf{I} - \mathbf{G_i}]^{-1}]\vec{E}_0(\vec{r}). \tag{2g}$$

The distortion tensor, $\mathbf{C}$, is therefore given explicitly in terms of the Greens' dyadics as

$$\mathbf{C}(\vec{r}) = \mathbf{I} + \mathbf{G}(\vec{r})[\mathbf{I} - \mathbf{G_i}]^{-1}. \tag{2h}$$

In general, the elements of this distortion or scattering tensor will be complex but in the limit for low frequencies they become dominantly real.

As a simple example, if the body is a hemisphere and the background field is a constant then the total electric field is constant inside the hemisphere when the vector potential (2b) contribution to the internal electric field can be neglected. The required dyadic $\mathbf{L}$ (2c) for an interior point is known to be (by symmetry from the solution for a sphere in a whole-space) $-\delta\sigma/3$ times the identity dyadic

I (Hohmann, 1976). Equation (2f) for the fields interior to the hemisphere then becomes

$$\vec{E}_i(\vec{r}_s) = \begin{pmatrix} \dfrac{3\sigma_b}{\sigma + 2\sigma_b} & 0 \\ 0 & \dfrac{3\sigma_b}{\sigma + 2\sigma_b} \end{pmatrix} \vec{E}_0(\vec{r}) = \mathbf{C}(\vec{r})\vec{E}_0(\vec{r}) \tag{3}$$

for any position within the hemisphere. The expression for the exterior scattering matrix, $\mathbf{C}(\vec{r})$, can then be derived using Equations (2h) and (2e). Although, these expressions can be derived directly from a scalar potential (Groom and Bailey, 1991), this development is instructive to illustrate how the scattering matrix **C** arises and under what conditions Equation (1) may break down.

Although, we have been able to justify the use of Equation (1) for scattering situations where the internal field is approximately uniform, only structures with specific geometrical symmetries have constant total internal electric fields. For the case of other geometries, a new first order approximation has been derived which can be regarded as an extension of the Born approximation (Habashy *et al.*, 1991). This approximation is extremely pertinent to the validity of Equation (1).

The Born approximation requires that the internal electric field be in-phase with the background field but does not account for the magnitude variation that can be caused by even moderate conductivity contrasts. This extended Born approximation is based on the fact that for a field point internal to the scatterer, $\vec{r}$, the Greens' dyadic (2a) is singular when $\vec{r} = \vec{r}_s$. For this case, it may be expected that the gradients of the Greens' dyadic are much larger than the gradients of the internal field. This assumption leads from (2a) to a linear approximation for the internal field from the background field

$$E_i(\vec{r}_s) = \mathbf{\Gamma}(\vec{r}_s)\vec{E}_0(\vec{r}_s) \tag{2f}$$

which is independent of the source characteristics but which is dependent on the scatterer geometry, the conductivity contrast and the position. In the low frequency limit, $\mathbf{\Gamma}$ is real and thus the internal field is in-phase with the background field but has a first-order correction for magnitude due to the charges caused by the conductivity contrast. Under this approximation, Equation (1) can be derived explicitly with only the assumptions that the frequency be sufficiently low to neglect the vector potential contribution to the internal electric field and that the background field be uniform over the scatterer. The approximation is indicated to be quite accurate (Habashy *et al.*, 1991) for most scattering problems which are relevant to magnetotellurics, although the approximation breaks down in cases where Equation (1) would not normally be expected to apply. That is, when there are large source field gradients over the scatterer, when the frequency becomes sufficiently high that inductive scattering within the inhomogeneity could not be

neglected, when the scatterer becomes many orders more conducting than the background and when the source is coupled with the body such that current channelling is negligible.

Effects of Small-Scale Scattering

The scattering effects of the distortion matrix, **C**, (1) are significant on the measured fields. It will, in general, mix the regional electric field components into the measured field components at the local site. If the background is two-dimensional and the TE and TM electric fields have different phases, then the measured field components will, in general, have a phase which is neither TE nor TM. The form of the distortion matrix, as a linear operator, will depend explicitly on the coordinate system in which it is expressed.

When the 3D body distorts the electric field from that of the background response, an anomalous current is produced which in turn produces an anomalous magnetic field. If the total electric field in the scatterer is in-phase with the background field then this anomalous magnetic field is in-phase with the primary electric field and thus can be described by a magnetic scattering matrix, **D**, (Groom and Bailey, 1991)

$$\vec{H}_a = \mathbf{D}\vec{E}_0. \tag{4a}$$

This result can also be seen from the integral equation representation

$$\vec{H}_a = \nabla \times \vec{A} = \nabla \times \int_{V_s} g(\vec{r}, \vec{r}_s)\delta\sigma\vec{E}(\vec{r}_s)\, \mathrm{d}v \tag{4b}$$

If the first term in (2b) is neglected in the scattered electric field, then the internal electric field and thus the scattering currents are in-phase with the background field. The components of the scattered magnetic field are therefore simply proportional to the vector dot product of the primary electric field vector with combinations of single derivatives of $f_A(\vec{r})$. Thus, even though the frequency may be low enough and the structure small enough to neglect induction effects of the small 3D scatterer, there may still be a contribution to the magnetic field from the galvanic scattering.

Structural Dimensionality and Invariants

It is convenient to first examine the effect of 3D scattering on traditional methods with the use of synthetic data. Here, we have used a regional structure which is two-dimensional (2D) and superimposed on the model a 3D hemispherical anom-

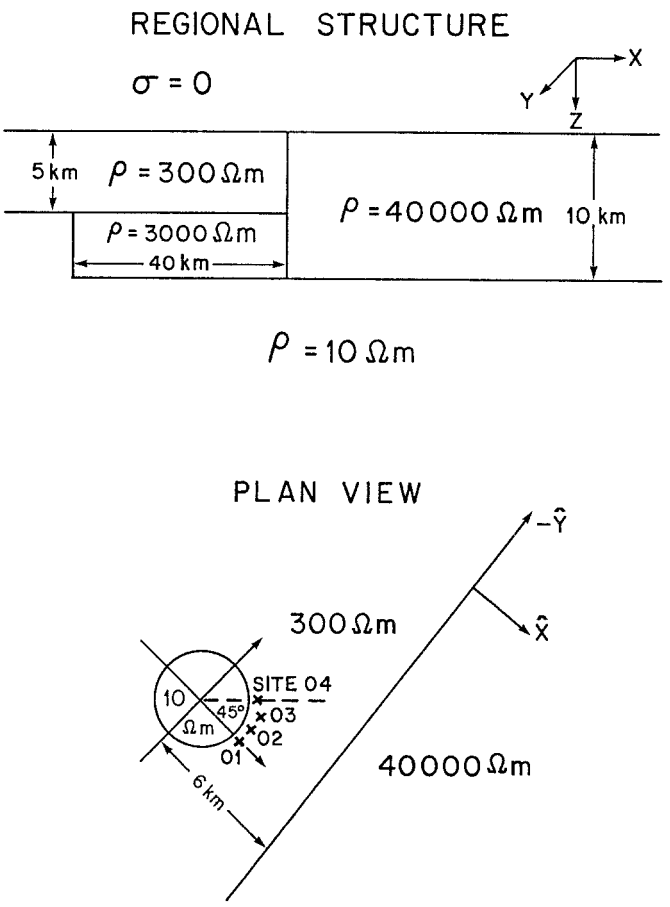

Fig. 1a. The regional two-dimensional model and superimposed 3D anomaly with measurement site locations.

aly (Figure 1a). (The true 2D response of the background is included in Figure 1b.) The hemisphere is sufficiently removed from the 2D boundaries so that the primary fields are essentially constant over the scatterer (verified numerically) so that the 3D electric and magnetic fields can be determined analytically as a function of position (Groom and Bailery, 1991). We take, as an example, the situation where the measurement axes are parallel and perpendicular to the 2D strike and the measuring position is outside the hemisphere at an angle of 30 degrees (Site 03 in Figure 1a) to the $\hat{x}$ measurement axes. To the synthetic responses, noise can be added to investigate the problem of parameter bias and resolution. The synthetic noise distribution used here is Gaussian with equal variance in all elements and mean zero. The noise is added such that N% noise means the variance is N% of the square of the magnitude of the largest impedance matrix element.

First, let us examine two commonly used 1D parameters; namely the square-

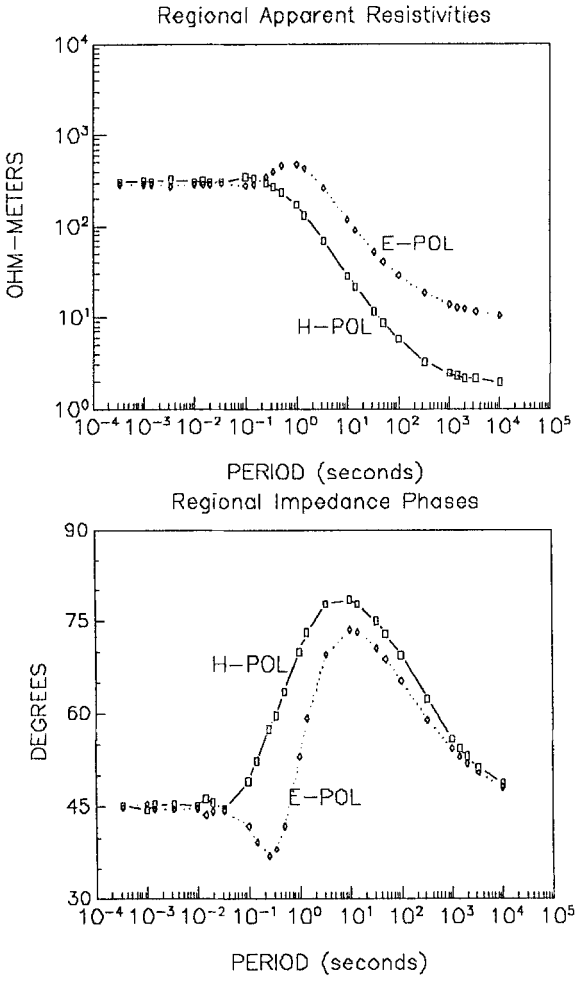

Fig. 1b. The regional responses as apparent resistivity and phase.

root of the determinant (called the "effective impedance") and the anti-trace or arithmetic average of the off-diagonal elements (called the "Berdichevsky average") (Berdichevsky and Dmitriev, 1976; Ranganayaki, 1984). The site is so situated that the determinant (Figure 2) is quite small due to the extent of current channelling. As such, the tensor becomes poorly conditioned and the effective impedance (DA) phase is badly determined in the presence of noise. Consequently, the 1D conductivity model generated from this parameter inadequately represents the true regional structure (Figure 1). The Berdichevsky average (BA) produces a more stable estimator with a fairly reasonable conductivity model (Figure 2). The adequacy of the inversion for the BA estimator over the effective impedance should not be construed as generally true but rather depends on the specific conductivity model. Note that the presence of the anomalous magnetic

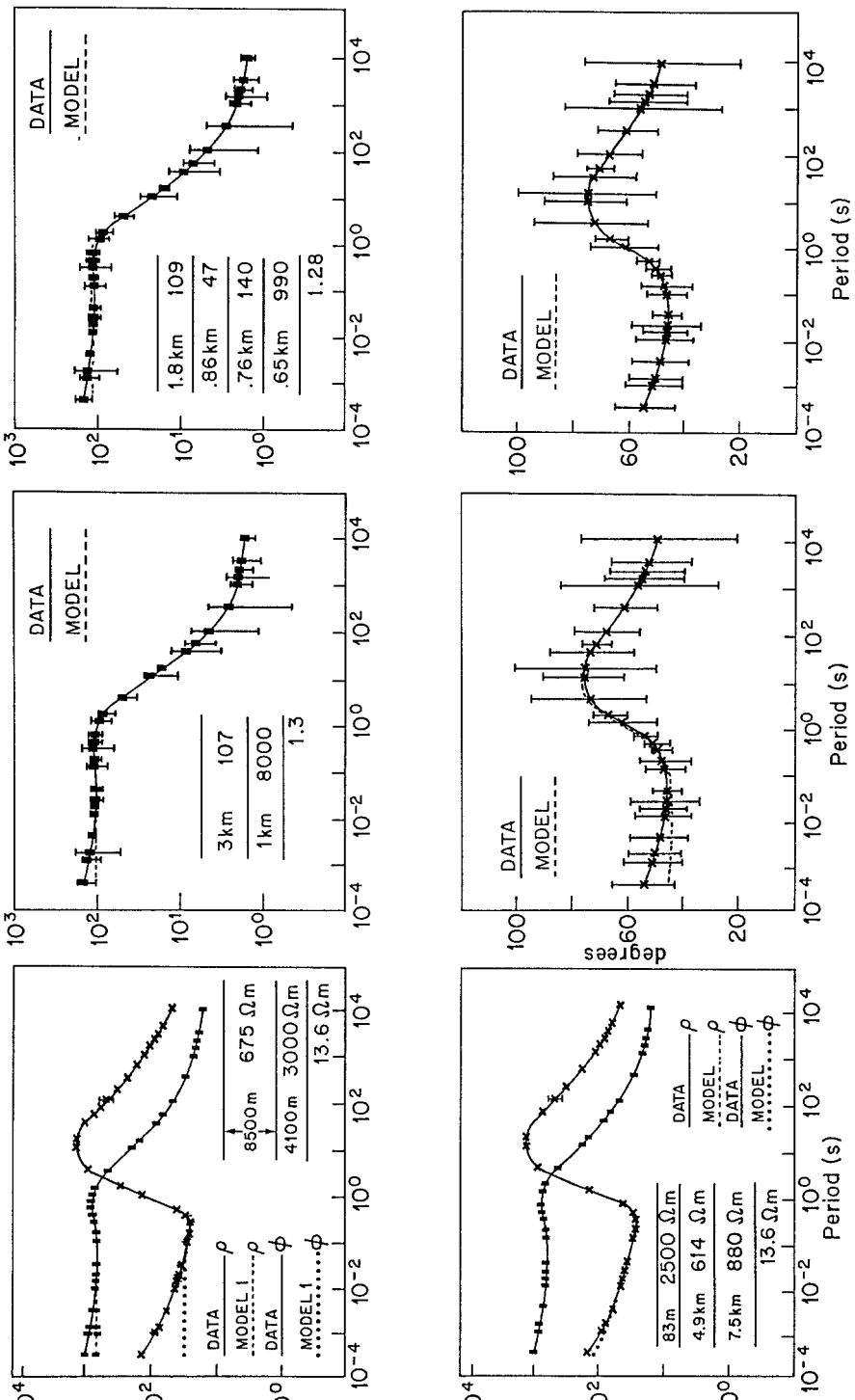

Fig. 2. The determinant (DA) and the Berdichevsky average (BA) estimators and their 1D inverses for synthetic Site 03. The left most figures (top and bottom) contain the BA and the inverse 1D model for a 3-layer model (top) and a 4-layer model (bottom). The middle figures contain the DA with 3-layer inverse (top: apparent resistivity, bottom: phase) while the right figures are the inverse and fit for a 5-layer model.

field results in a frequency-dependent phase perturbation at the higher frequencies for both these estimators. This perturbation requires that a fictitious thin resistive surface layer be included in the 1D conductivity structure to fit the data. In experimental situations when the structures are very large, the 3D response may not be significant until longer periods with the result that the phase perturbations due to the anomalous magnetic effects could result in additional layers being included at some depth.

Next we examine a traditional 2D rotation parametrization of the data (Swift, 1967). Figure 3 contains 6 conventional parameters from this method (skew plus the 5 parameters previously mentioned) for the same site as above. Groom and Bailey (1991) discuss many points regarding the figures but we summarize only a few. The strike direction should be either 0 or 90 degrees, but is incorrectly determined by this method. Rather the estimate of the strike angle at short periods is the azimuthal position of the site. (The local current azimuth or direction of current channelling is determined primarily by the local structure when the 3D scattering is severe. If the background is 1D then this current azimuth must be the azimuth of the site for such an isotropic structure (Groom and Bailey, 1991).) At mid-band periods, the strike estimate undergoes a frequency-dependent transition to a long period asymptote. This transition takes place over just those periods where the regional structure has its largest inductive response. Under this 2D parametrization, strong 3D static effects mean the strike direction is usually a function of the local site geometry and thus the local current channelling. The recovered impedances are mixtures of the two regional responses. This can be seen most obviously in the phases but also in the shapes of the apparent resistivity curves.

The reader will note that the error bars sometimes are not centered about a data point in these figures. In most cases, the parameters are nonlinear functions of the impedance data. As such, the presence of noise will not only scatter the value of a parameter as in a linear system but will also bias the result. Thus a parameter derived from data with noise will tend to be scattered about a point removed from the value of that parameter when no noise is present. That is any amount of noise could cause the parameter estimate to be biased consistently in one direction (up or down). In these plots, the scatter in a parameter is determined in an empirical fashion. Noise is added to the data then the parameter determined; a different noise realization added and then the parameter redetermined and so on for a set of N noise realizations. The scatter of the parameter is then examined from the set of realizations and this scatter is plotted as an error bar. In this way, it can be seen that some parameters are easily biased by noise whereas others are relatively unbiased.

We use here a non-conventional parameter (i.e. Figure 3); the residual between the estimated impedance tensor, $\hat{\mathbf{Z}}$, and the actual measured data, $\mathbf{Z}_m$, (Groom and Bailey, 1989a),

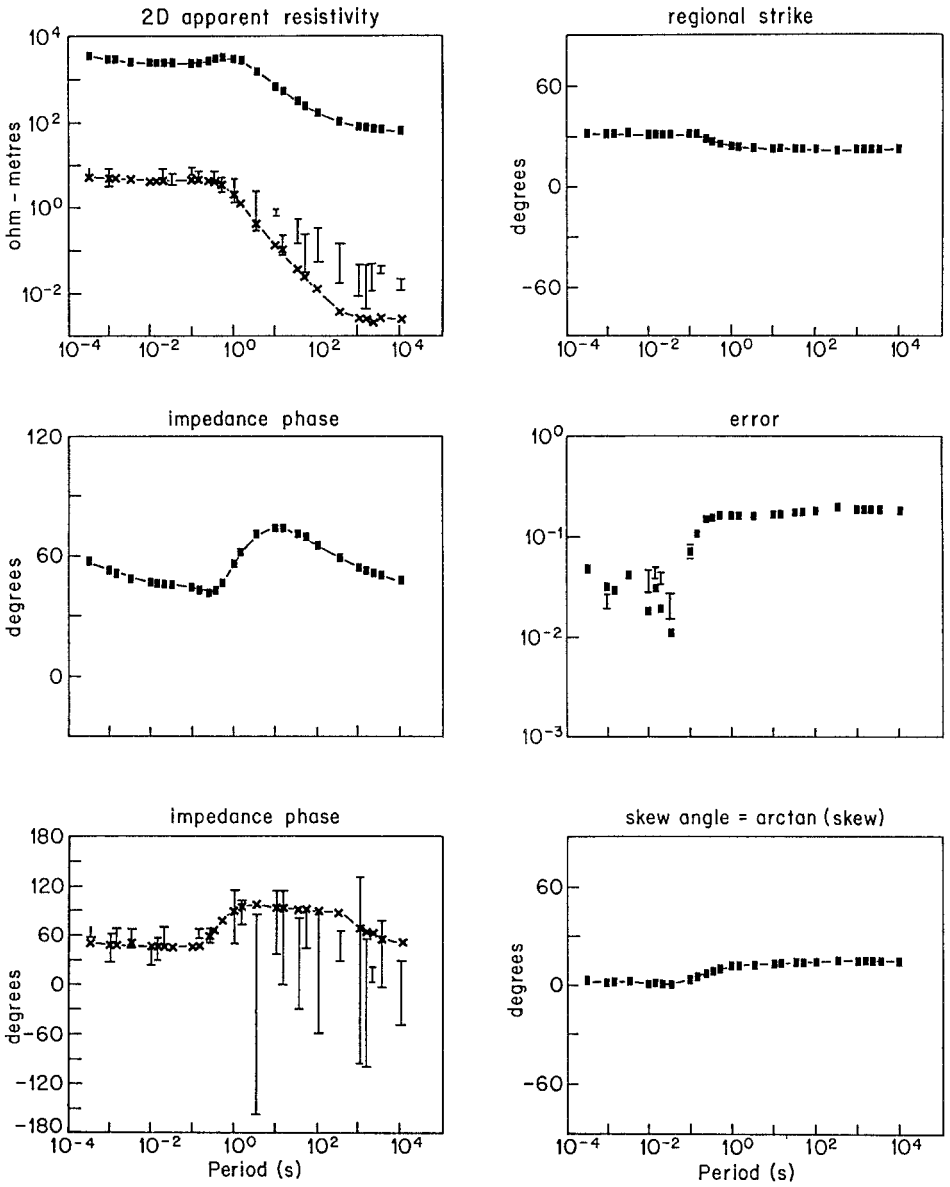

Fig. 3. Traditional 2D rotated decomposition of Site 03. Apparent resistivity estimates are plotted on same subplot while phase estimate plots are plotted separately. Strike estimate, skew and a residual are also plotted.

$$\epsilon = \|\hat{\mathbf{Z}} - \mathbf{Z}_m\|. \tag{5}$$

With a two-dimensional model, for example, the estimated tensor would be a rotation of a tensor with zero diagonal elements. The rotation angle being the recovered 2D strike estimate while the off-diagonal elements are the estimated

TE and TM impedances. In Figure 3, a simple least squares norm has been used which is normalized by the magnitude of the elements of the measured data so that it will lie between 0 and 1. If the residual is acceptable it should be less than the noise level (here 0.04). At short periods, the residual is acceptable but grows to an unacceptable level at long periods. The residual is acceptable at short periods because the conductivity structure is 3D locally and 1D regionally while at longer periods it becomes 3D-2D and because the 3D structure is rotational invariant in the z-axis and thus **C** for this structure is a symmetric operator. The use of a residual statistic is essential in the examination of the applicability of models to the data. Since the variance is equivalent for all 4 elements of this synthetic data tensor, the least squares norm is equivalent in this case to a chi-square type norm where the differences in the data element and the estimated tensor are inversely weighted by the variance in this data element. It is not obvious what norm should be used for defining the residual statistic, although one of the authors (RG) uses a chi-square normal for almost all data analysis. Figures 5–7 utilize the chi-square norm.

Mathematically-Based Decompositions

Over the last decade, a number of attempts have been made to develop useful MT tensor decompositions which are mathematically motivated. These decompositions are based specifically on a mathematical treatment of $\mathbf{Z}_m$ as a complex rank 2 tensor rather than a formulation of $\mathbf{Z}_m$ as a response function that links the measured fields in the presence of 3D scattering. Although the most comprehensive of these investigations is present in Spitz (1985), we will briefly examine Eggers' (1982) eigenstate decomposition as the first such method and refer the reader to Groom and Bailey (1991) for a more detailed discussion of others and their comparisons. The *eigenvalues* of Eggers' decomposition are not the traditional eigenvalues of a rank 2 tensor but are defined via a matrix which rather than being diagonal has zero diagonal elements (sometimes referred to as anti-diagonal). The eight parameters of Eggers' decomposition are the magnitude and phase of the complex eigenvalues, the orientations of the major axes of the electric eigenvector polarization ellipses and their respective ellipticities. As previously, we again use the synthetic 3D data to examine Eggers' decomposition and reiterate that these data represent only a single 3D scatterer and there are no inductive effects associated with it.

In Figure 4, the complex eigenvalues of the impedance tensor are displayed as scaled magnitude and phase. The orientations and ellipticities of the eigenvectors are also plotted. Eggers (1982) states that the eigenvalues are the 2D rotated impedance estimates when the structure is 2D. Stated in another way, if one assumed the structure was 2D and determined the impedances algebraically then one would obtain the equation for Eggers' eigenvalues. (When the structure is

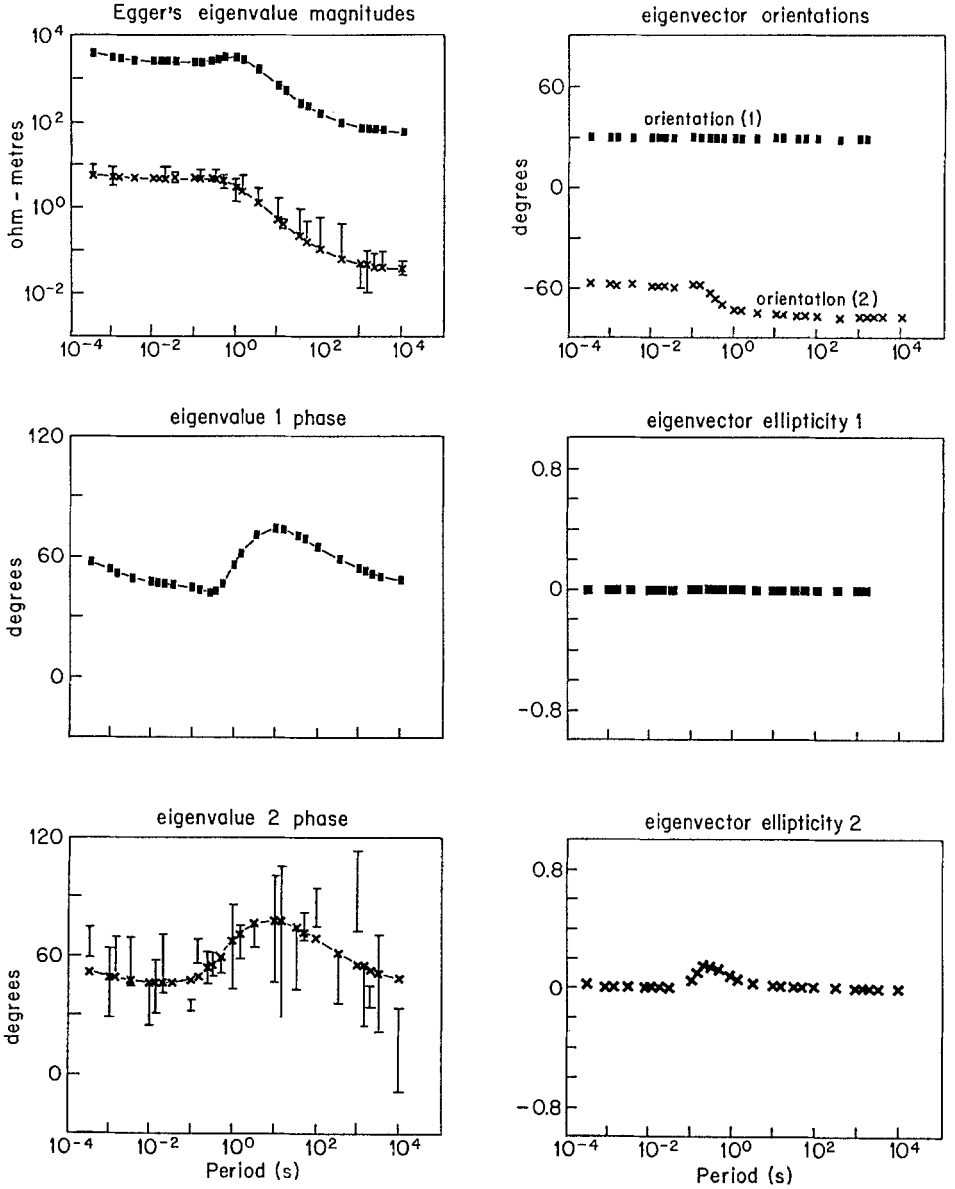

Fig. 4. Eggers (1982) eigenvalue magnitudes and phases are plotted for Site 03 along with eigenvector orientations and ellipticities.

2D, algebraic methods produce stable rotationally-invariant estimates of the 2D impedances independent of the strike estimate which can be unstable at high noise levels.) How similar are the algebraic eigenvalue estimates of impedance and the traditionally rotated estimates when 3D scattering is significant? Figure 4 shows clearly the mixing of the regional responses in the eigenvalues. In fact, close

comparison of Figures 3 and 4 indicates that the major impedance estimates by the eigenvalue method and the conventional 2D rotation method are virtually identical. The minor estimates are also extremely similar until the minor estimate from rotation becomes unstable due to noise. This similarity between Swift's and Eggers' methods is the same for any site inside or outside the hemisphere. The implication being that under such 3D responses, the rotated 2D estimates are essentially the eigenvalues. However, estimation of the minor eigenvalue by a rotation method may be unstable. A rotationally invariant algebraic estimate will be generally preferred.

We now turn to the eigenvector characteristics. At this site, one eigenvector orientation is very constant about 30 degrees (the site azimuth w.r.t. the coordinate system, Figure 1a) while the other begins perpendicular but undergoes a transition much like the 2D strike estimator (Figure 3). These orientations are much more closely related to the local current channelling than any regional inductive response and as such are locally site specific in 3D environments. One ellipticity is essentially zero while the other is non-zero only through the 2D inductive range. This ellipticity information may be useful as channelling-induction indicators when fully understood.

The LaTorraca *et al.*'s (1986) produced no significant variation from these results. The skew angle for this method provided no further information beyond the traditional skew. One of the decompositions of Spitz (1985) is essentially equivalent to those of the two aforementioned authors for these scattering conditions, while the other of Spitz's two decompositions is very similar to a technique developed by Yee and Paulson (1987). Although, the latter two methods appear to offer the possibility of recovering information about the regional responses (Groom and Bailey, 1991), the methods have not yet been understood nor developed to utilize them in normal processing circumstances.

Useful application of the mathematical decompositions is, however, restricted for reasons other than those discussed. These techniques do not address the occurrence of level shifts of the eigenvalue magnitudes. This level, or "static", shift can be seen by comparing the eigenvalue magnitudes of Figure 4 with the *correct* or regional magnitudes shown in Figure 1b. We will return to this level problem below with regard to the physically motivated decompositions.

Physically-Based Decompositions

In this section we consider decomposition techniques that yield more obviously physically meaningful parameters (e.g. regional strike and regional impedances) rather than mathematical parameters (e.g. eigenvalues) which are, as yet, not so readily interpretable. The first physically based decomposition was introduced by Larsen (1977). The model consists of a local, small-scale 3D anomaly over a

layered earth. In this case, the assumed form of the impedance tensor can be derived from (1) as

$$\mathbf{Z}(\omega) = \begin{pmatrix} C_{xx} & C_{xy} \\ C_{yx} & C_{yy} \end{pmatrix} \begin{pmatrix} 0 & Z_n(\omega) \\ -Z_n(\omega) & 0 \end{pmatrix}. \tag{6}$$

Z_n is the normal impedance of the layered earth. The distortion matrix elements, C_{ij} are taken to be real and frequency-independent at sufficiently low frequencies for which the inhomogenous top layer is thin compared to the penetration depth. Therefore, all elements of the measured tensor must have the same phase if they are to be explained by Equation (6). Larsen extended this model to include the possibility of a magnetic field associated with the current channelling as discussed above (Equation (4)). Although the factorization was general, Larsen's algebraic method of decomposition was limited to distortion or scattering matrices of only a certain form which may be categorized as being for the case of weak scattering (Groom and Bailey, 1989a).

If the regional conductivity distribution is two-dimensional then more than one phase can occur in the tensor (Bahr, 1988). Extending Equation (6) to include the possibility of two regional 2D impedances and the possibility of a magnetic field associated with the galvanic scattering, we obtain (Groom and Bailey, 1991)

$$\mathbf{Z}(\omega) = \mathbf{R}(\theta)\mathbf{C}[\mathbf{I} - \mathbf{Z}_2(\omega)\mathbf{D}]\mathbf{Z}_2(\omega)\mathbf{R}^t(\theta). \tag{7a}$$

Here the scattering matrices, **C** and **D**, are defined in the natural or intrinsic co-ordinate system of the underlying 2D structure defined by the 2D strike. $\mathbf{R}(\theta)$ is a rotation operator, **I** is the identity matrix and $\mathbf{Z}_2(\omega)$ is the background or 2D off-diagonal impedance tensor expressed in the strike co-ordinate system. Notice that the electric distortion matrix, **C**, is assumed real while the magnetic distortion operator on the impedances, $[\mathbf{I} - \mathbf{Z}_2(\omega)\mathbf{D}]$ is clearly complex and frequency dependent. The electric effect causes a mixing of the 2D regional impedances whereas the magnitude effect causes mainly phase distortions. The magnetic distortion decays with decreasing frequency approximately as $\sqrt{\omega}$.

One important problem associated with conventional 2D methods and the mathematical decompositions is that often the regional responses will be mixed in the impedance tensor when there is galvanic 3D scattering. Once the tensor is rotated, the impedance tensor elements can reside in any of the four complex quadrants with the result that if the tensor is studied in the wrong co-ordinate system the phases of the impedances may seem to extend outside normal bounds. As an example, a data set is chosen from the 1987 Lithoprobe survey in the Canadian Cordillera. This site is situated in a valley which follows a major fault (Slocan Lake Fault). If one examines the data in a geographic (NS–EW) co-ordinate system (the measurement axes), then the phases of the EW impedance extends beyond expected 0–90 degree bounds up to more than 180 degrees (Figure

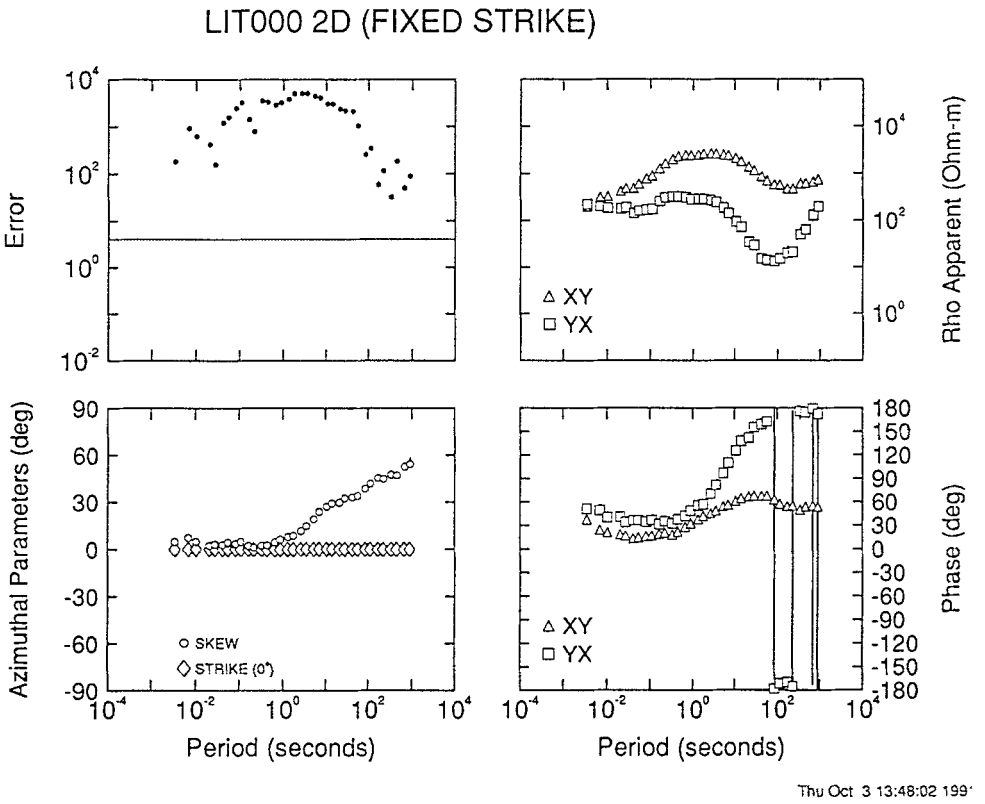

Fig. 5. Off-diagonal elements of experimental data at Site 000. Skew angle is plotted along with strike in lower left. A residual error is also plotted. Here it indicates the relative importance of the diagonal elements versus their variances.

5). (Here a negative is removed from the Z_{yx} element as a convention). The other subplots are the apparent resistivity, a normalized χ^2 error of fit (Groom *et al.* (1991)) and a plot showing the strike angle and the conventional skew as an angle (arctan of skew). Note how the skew rises to large values as the phase extends out of the predicted quadrant. The next figure (Figure 6) illustrates the data decomposed via a traditional rotated method. Notice again how the *YX* phases rise out of the predicted coordinate system. The strike estimate is aligned with the strike of the valley at short periods but asymptotes to zero degrees (the measurement axes) at long periods. The synthetic results (e.g. Figure 3) indicate that a combination of strong local 3D current channelling and strong 2D current channelling can result in a long period asymptote for a strike estimate from a 2D assumption that is neither the local direction nor the regional direction. In fact, this is the first clue that there may be an underlying almost 2D strike on a large scale.

Rotation of the data to another co-ordinate system can produce better behaved

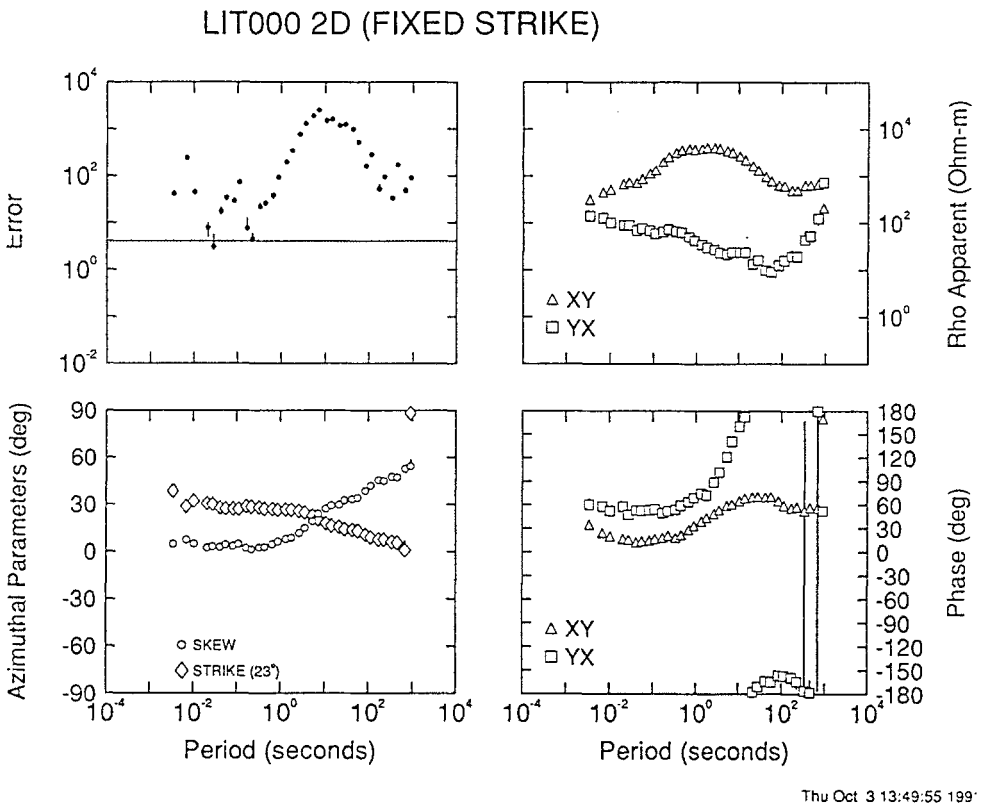

Fig. 6. A traditional 2D rotated decomposition of experimental site 000.

phase responses. For example if the data are rotated to 30 degrees East of North (Figure 7) then both impedance phases are considerably better behaved. Is there any physical meaning to this azimuthal direction of 30°?

These results suggest the presence of strong 3D effects on the measured electric field. We therefore utilize a galvanic distortion decomposition first introduced by Bahr (1988) in an attempt to separate the phase and apparent resistivity responses of the background and find the correct co-ordinate system. Bahr combined Swift's (1967) and Larsen's (1977) model. The model is a small 3D anomaly within a 2D Earth with the governing equations being simply (ignoring magnetic effects)

$$\mathbf{Z}(\omega) = \mathbf{R}(\theta)\mathbf{C}\mathbf{Z}_2(\omega)\mathbf{R}^t(\theta) \tag{7b}$$

where $\mathbf{Z}_2(\omega)$ is a regional off-diagonal tensor. Various parameters are recovered by decomposing the tensor data under this model. The recovery of these parameters is generally a non-linear inverse problem (Groom and Bailey, 1989a).

We will illustrate our discussion of such a decomposition with the synthetic and experimental data previously used. We will utilize the decomposition method of Groom and Bailey (1989), although the general results will be similar for all such

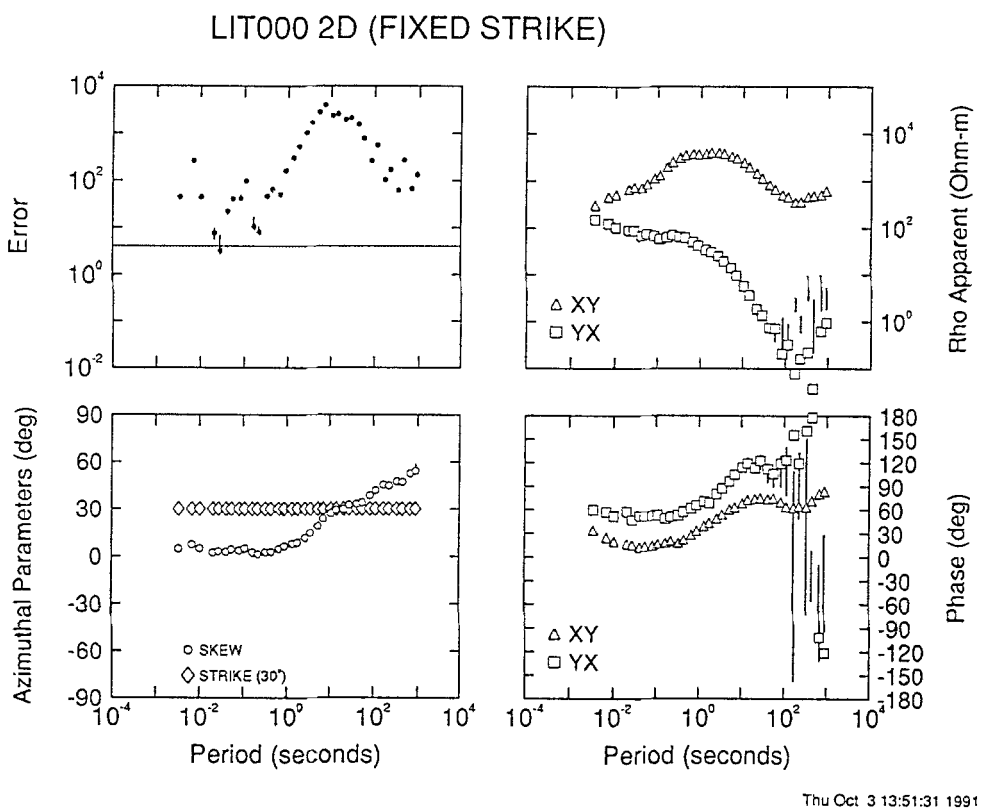

Fig. 7. The experimental data at site 000 rotated and assumed 2D at a strike angle of 30 degrees. Notice the reduced residual from previous plots for the shorter periods and the more well behaved phase estimates.

decompositions. This method is based upon a general subfactorization (not SVD) of the electric distortion matrix into 3 constituent parts and then a non-linear minimization to determine a subset of the parameters.

As we now have available four physically based decompositions, or models, from 1D up to subsets of 3D, we would like to treat the decomposition as a type of inverse problem. As we move to higher dimensional models, we introduce more parameters. Thus, we must not only examine the residual between estimated data and measured data but whether a reduced residual is simply due to an increase in the number of model parameters (or "roughness"). In addition, we wish to know the resolution of a particular parameter in any given decomposition. It is important to understand that the extent of the current channelling can severely affect the ability to invert the tensor data. If there is extreme current channelling, then the local current is forced to flow along a specific direction independent of the source polarization (class 6 type distortion, Bahr 1991). That is, the local electric field lives in a one-dimensional vector space whereas the background electric field and

magnetic field live in a two-dimensional space. As such, **C** and thus **Z** are singular for their rank is only one. This then becomes an ill-posed inverse problem if no *a priori* constraints are made. An examination of the eigenvalues, as initially suggested by Eggers (1982), is therefore extremely useful as a precursor to any analysis.

To illustrate these points, let us examine the effect of noise on the resolution of the true regional strike under the 3D model. This is probably the most fundamental problem associated with 3D near-surface effects on MT data. To illustrate effectively we have rotated the data 30 degrees counterclockwise to a different measurement axes. Figure 8 (bottom right) contains a contour plot of the residual (normalized chi-square) as a function of period and regional strike for the synthetic data. (The noise for this first result is extremely small; just sufficient to dominate computer machine noise.) In this figure, below -1.0 indicates a good fit while about 3.0 indicates an unacceptable fit. At short periods, there is little indication of a preferred strike due to the fact that the site is too far removed from the 2D lateral contacts to sense them at these periods (Figure 1a). In other words, at short periods the structure is approximately 3D over 1D. In the mid-band, the preferred strike is a fairly narrow strip about 30 degrees (true regional strike) while in the long periods the strike again is not so well determined. This latter result is due to the fact that there is essentially only one regional phase at long periods as the 2D structure is now simply a thin-sheet. Thus we see that the strike at long periods, can no longer be resolved within the noise. The same figure (bottom left) also shows the same information but now 4 per cent noise is added albeit in a severe manner. Notice that the strike cannot be resolved at all except possibly in that band where the 2D induction is strong and even here the resolution is not particularly narrow. This is due, to a great extent, on the severe current channelling which poses a problem for any inverse parametrization.

The distortion parameters, however, are more stable in the presence of noise (right Figure 8). Here the shear is contoured as a function of strike and period for the low noise (top right) and high noise (top left) data sets. Using this information and seeking a smooth (fewest parameters) model, one attempts to obtain the best parametrization as a trade-off between the degree of roughness (number of parameters) and the residual. For example, one would generally desire a strike direction which was consistent with a direction resolved from the residual plot over a part of the period band in combination with the fewest distortion parameters (i.e. fixed over a period band). A strike of near thirty was consistent with both requirements. For the high noise, the preferred strike was weakly defined as less than 30 degrees. For these angles, only an angle near 30 degrees allowed for frequency-independent distortion parameters. Fixing the strike at thirty degrees and letting the remaining parameters be free resulted in the parametrization shown in Figure 9 for the noisy data (measurement axes rotated back to original for comparison to earlier figures). The distortion parameters are without constraint

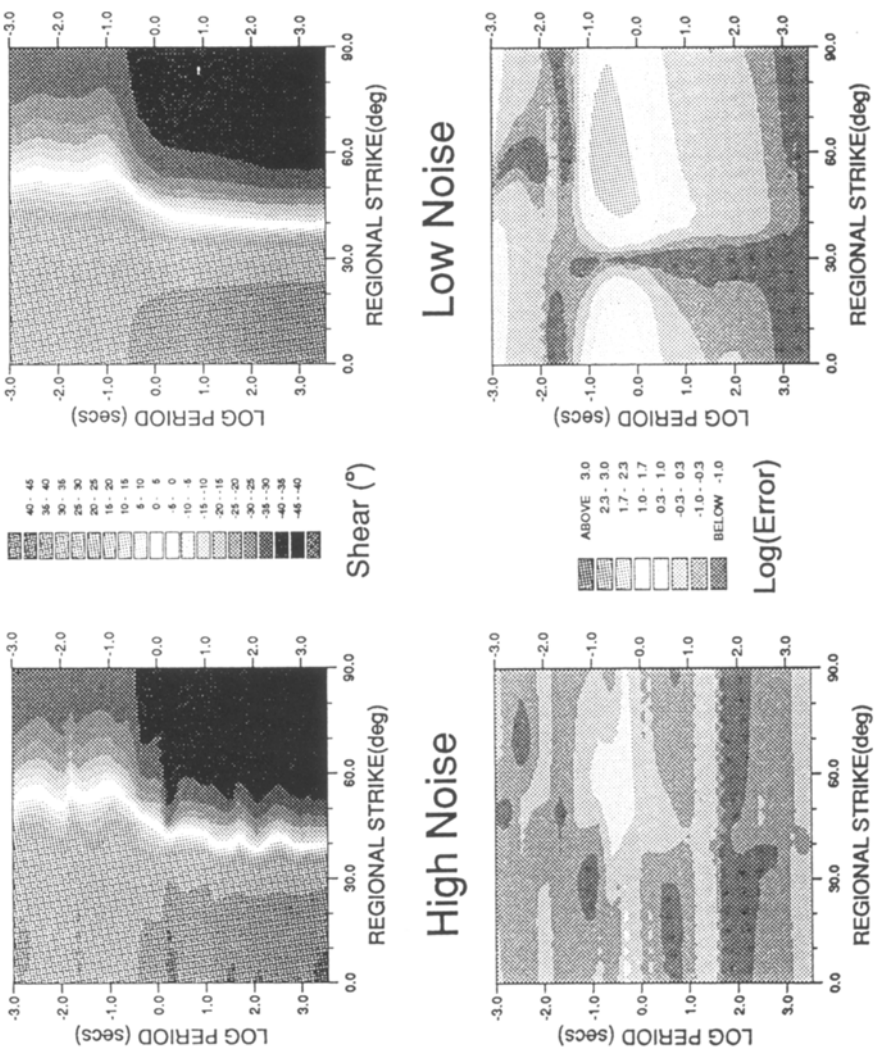

Fig. 8. Decomposition parameters for Site 03: Contoured chi-square residual and shear as functions of assumed strike angle for two levels of signal noise. Top: shear angle, bottom: residual, Left: High noise, Right: Low noise. Data rotated 30 degrees counterclockwise.

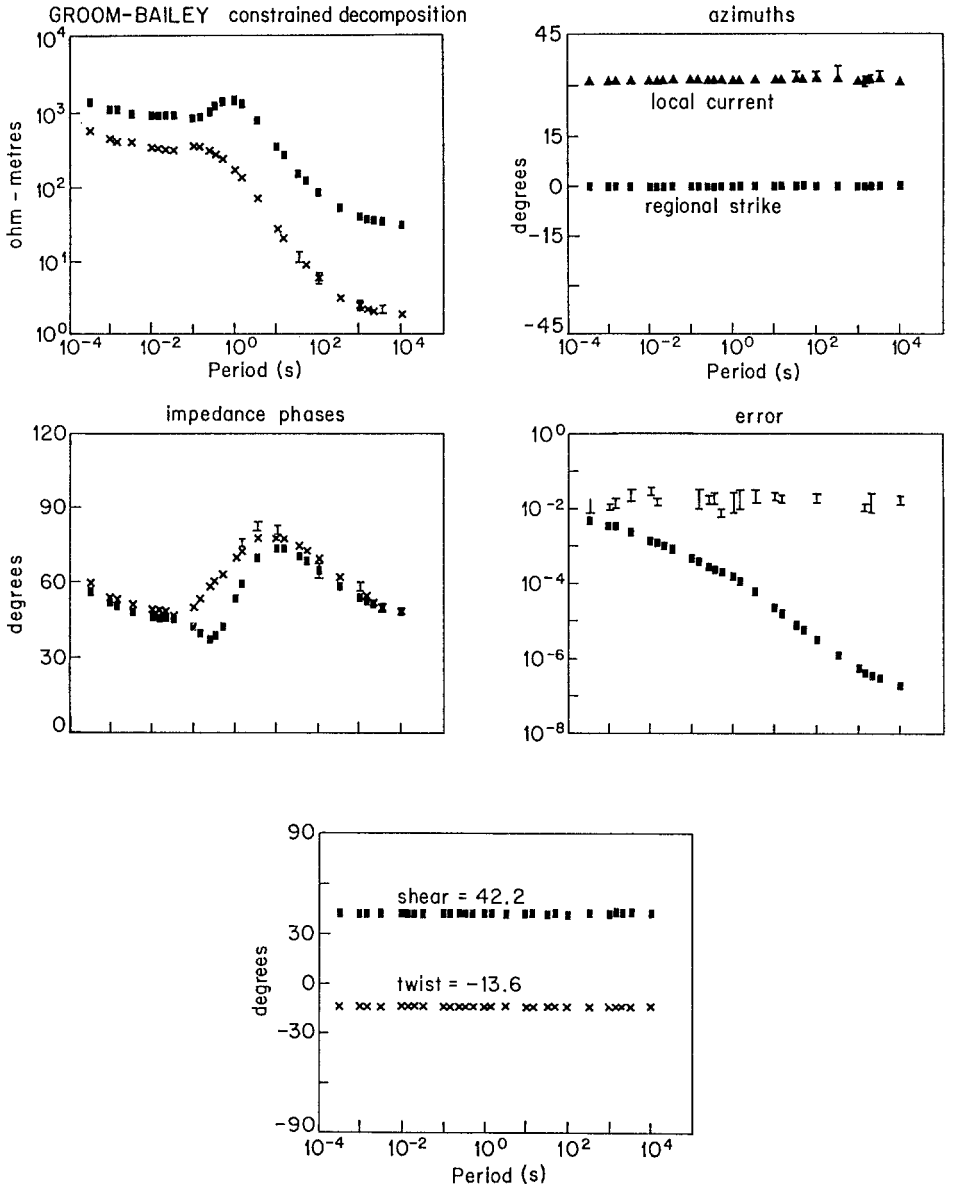

Fig. 9. Strike constrained Groom–Bailey (1989) decomposition for synthetic data at Site 03. Regional impedance estimates, regional strike, local current azimuth estimate, L2 residual and the two removed 3D factors (twist and shear) are plotted.

quite constant. They can now be fixed to produce a model which requires $4N + 3$ parameters where N is the number of periods. The residual is at the correct level at about 0.04.

Having satisfied our requirements of minimizing the residual while having the

fewest azimuthal parameters (strike plus distortions parameters), we now investigate whether we have accomplished our objective of recovering the true regional impedances. The impedance phases are now unmixed and fairly well resolved (Figure 9). For periods shorter than 0.01 seconds, they still retain phase effects of the currrent channelling but below this period they are extremely close to the true regional phases (Figure 1b). The true shapes of the regional apparent resistivity curves are obtained with only slight high frequency modification from the galvanic magnetic effects. The previous strike angle analysis indicates that the magnitude splitting at short periods between the recovered TE and TM modes is due to the near-surface structure and not the larger 2D structure. The splitting that remains is due to a diagonal operator (local anisotropy) (Groom and Bailey, 1989a) which can always be written in the form:

$$\mathbf{A} = g\begin{pmatrix} 1-s & 0 \\ 0 & 1+s \end{pmatrix}.$$

The factor s (local anisotropy) can often be estimated algebraically from the short period data and then removed from the entire period range particularly when the non-1D, high frequency scattering is not of interest to the investigator. Thus, the current relative level between the apparent resistivities can often be found but the one mutual static shift (g, site gain) is more difficult. This final shift is most severe inside or on an outcropping anomaly, much decreased immediately outside the 3D scatterer while decaying rapidly to 1 with increasing distance from the anomaly.

The problems of analysing 3D data with 2D models, as seen by the use of synthetic data, relate directly to actual experimental data. Examination, for example, of the earlier experimental data indicated that while the data were near 2D at higher frequencies following the strike of the valley, the data became strongly 3D by 1 second. This is a common problem. Data are often collected along valleys where access and instrument deployment is reasonable. However, the sediments in the valley often provide good gatherers of current so that at long periods there are strong 3D current channelling effects when the valley is no longer long enough or straight enough to be approximated two-dimensionally. In this case, the current channelling was so severe constraining the current along 30 degrees East of North (this is the physical meaning associated with this azimuth as mentioned above) that it was difficult to resolve the regional strike within the noise levels. A neighbouring site some 15 kilometers to the West had less severe 3D effects and indicated an underlying strike of 60 degrees East of North at periods longer than about 1 second after decomposition. Applying this strike to the decomposition of this data provided a good fit, well resolved phases and long period phases which matched those at the neighbouring site. This process was carried on for sites along a profile of more than 150 kilometers (Jones *et al.*, 1988) most of which had strong 3D effects especially at long periods. Figure 10 compares the phases recovered

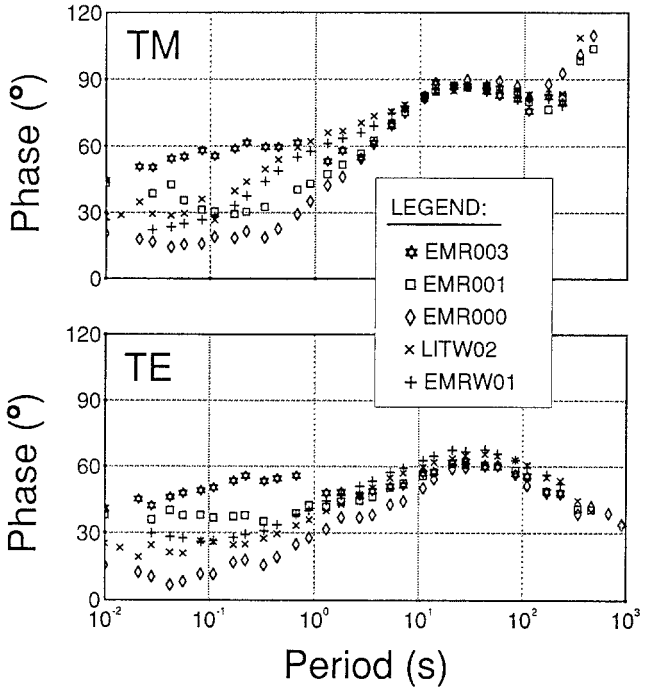

Fig. 10. Regional Phases: Comparison of regional phases after decomposition for 5 experimental sites near site 000 (here termed EMR000). Note the extreme similarity of the long period TE and TM phases at all sites thus giving confirmation to the analysis.

after decomposition from a number of these sites each separated from each other by about 10–15 km E–W.

Static Shift as a Sub-Problem of Decomposition

The decomposition (7b) involves a real 2×2 distortion matrix **C**: Its four elements determine the two ways in which electric fields are modified by small-scale local conductivity anomalies. The normalized off-diagonal elements of **C** describe angular deviations of the regional electric fields. In fact, if the impedance tensor has been transformed into the coordinate system of regional strike then the expressions

$$\beta_1 = \tan^{-1}\left(\frac{C_{xy}}{C_{yy}}\right) \qquad \beta_2 = \tan^{-1}\left(\frac{C_{yx}}{C_{xx}}\right) \tag{8}$$

determine two angles (Figure 11), which describe, how much the two electric fields associated with TE and TM modes of the regional 2D anomaly are *rotated* out of their normal directions. Bahr (1991) shows that these angles can either be calculated from the decomposition parameters *twist* and *shear* of Groom and Bailey

$$\underline{\underline{Z}} = \underline{\underline{C}}\,\underline{\underline{Z}}_2 = \begin{pmatrix} c_{xy} Z_{\parallel} & c_{xx} Z_{\perp} \\ c_{yy} Z_{\parallel} & c_{yx} Z_{\perp} \end{pmatrix}$$

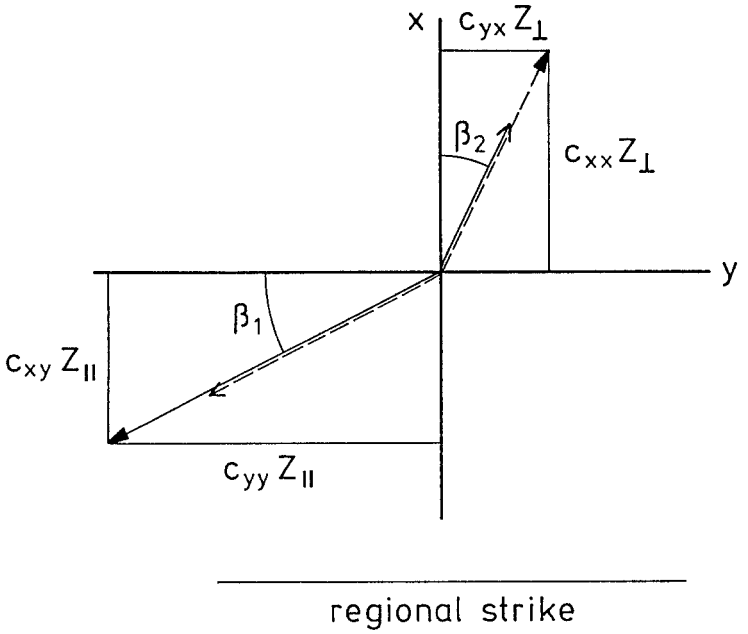

Fig. 11. Angular deviations of the regional electric fields plotted in the co-ordinate system of the regional strike.

(1989a) or directly from the elements of the measured impedance tensor after decomposition.

While the ratios (8) are accessible, two other distortion parameters remain which describe amplifications of the two electric fields associated with the TE and TM modes of the regional 2D anomaly. These factors are often referred to as *static shift* factors. It is important to point out that even the physical decomposition techniques of Bahr (1988) and Groom and Bailey (1989) do not solve the problem of static shift but rather allow for a possible application of an additional static shift removal technique.

The conductivity model for the most complicated physical decomposition incorporates a superposition of a regional 2D and a local 3D anomaly. For a single frequency, the regional anomaly is sufficiently described by up to 5 parameters, that is, the regional strike as well as the 2 phases and the 2 apparent resistivities. It is assumed that the effect of a local anomaly is described by the 4 real elements of the distortion matrix **C**. A 10th parameter is required that addresses the residual

problem referred to above. As any measured impedance tensor provides only 4 complex impedances, it would seem that a smaller set of parameters must be calculated in order to obtain a unique inverse. Of course, in some situations not all 8 data in the tensor are independent. For example in the 1D background case, there are at most 6 parameters constituting the model. Also, since some of the parameters are assumed frequency-independent, such as strike and the elements of **C**, it may initially appear that multi-frequency inversion might allow for a unique inversion for the entire set of 10 possible parameters. However, part of the non-uniqueness is determined by the basic physics. The local anisotropy and the regional anisotropy cannot, in general, be separated without additional information (Groom and Bailey, 1989a).

Generally, there still remains two unaccessible frequency independent parameters. In the context of physical decomposition, we can describe these two unaccessible parameters by combinations of elements of the distortion matrix **C**:

$$D' = (C_{xx}^2 + C_{yx}^2)^{1/2}, \qquad D'' = (C_{xy}^2 + C_{yy}^2)^{1/2}. \tag{9}$$

These expressions can be derived directly from Equation (7b) when expressed in the regional coordinate system. These parameters describe how much the amplitudes of the two electric field components are modified from the underlying response. In terms of the Groom and Bailey (1989a) decomposition, the two parameters are combinations of the scalars, g (the so-called site gain), and s (the local anisotropy). In the case of the 1D decomposition of Larsen (1977) only the site gain could not be identified uniquely. If the background is 1D, then the local anisotropy in the Groom and Bailey method can be recovered but again the site gain cannot be determined uniquely.

The following sections summarize some of the techniques that have been used to estimate the one or the two static shift factors with respect to some additional information besides the single site tensor data. These techniques are reviewed by Singer (this volume). Here we only intend to study their usefulness in the presence of complicated local conductivity structures which require both a decomposition and a static shift removal technique. Nevertheless, we want to point out clearly that so far none of these static shift removal techniques have been proven to work well in every geological environment.

Modelling C by the Use of Additional Information about the Surface Layer

This method provides an independent check of the near-surface conductivity as well as the geometry of local structures by use of some rapid geoelectrical mapping technique. The resulting resistivities may provide the input for a forward modelling with some DC or thin layer model. That model then hopefully yields the elements of the distortion matrix **C**.

In particular, bimodal thin layer models may account for both angular deviations

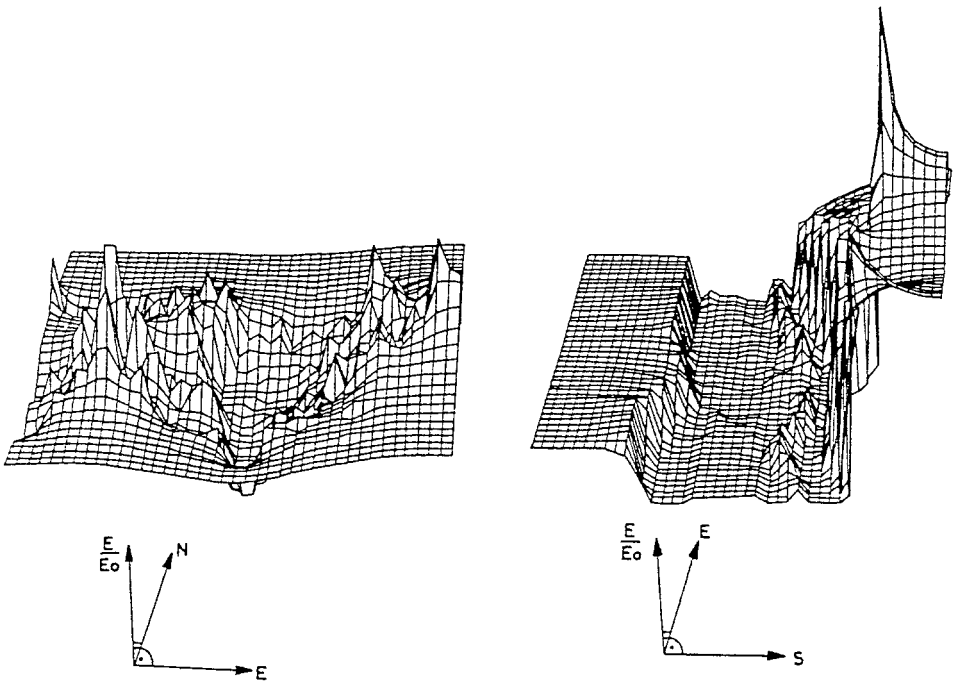

Fig. 12. Distortion matrix parameters c_{yy} (left) and c_{xx} (right) as calculated from a DC model (Kemmerle, 1977).

and amplifications of the telluric field. In theory, they can provide a complete distortion tensor rather than a scalar distortion factor. As an example, Figure 12 presents Kemmerle's (1977) results of the C_{xx} and C_{yy} distortion matrix elements as a function of location. A constraint of the mapping technique is that if the extension of the local structures is unknown, the geoelectrical mapping has to cover a very large area, requiring extremely time consuming field procedures. The distortion matrix, **C**, can vary greatly depending on the specifics of the 3D local structure.

Alternatively, the resistivity obtained with some geoelectrical or TEM technique at a single point can simply be used to fix the correct position of the high-frequency MT curves (Sternberg *et al.* (1988), Pellerin and Hohmann, 1990). Spies (1989) showed that there can be an overlap in the depth of investigation of the TEM and the MT method. In contrast to the mapping technique mentioned above, only a scalar factor is found. Craven *et al.* (1990) experimenting with these techniques with large data sets had little success.

All techniques mentioned in this section reveal a distortion factor or distortion tensor for some high frequency band of the MT sounding curves. These factors can be applied only with great care to the low frequency band of the curves if

additional 3D scattering occurs at greater depths: At sufficiently low frequencies, experimental impedance tensors often have the form

$$\mathbf{Z} = \mathbf{C}_u \mathbf{C}_d \mathbf{Z}_n. \tag{10}$$

Here $\mathbf{C}_u$ and $\mathbf{C}_d$ refer to distortion tensors which are related to surface and deep conductivity anomalies, respectively. Only $\mathbf{C}_u$, of course, is addressed with the surface layer techniques. Determination of $\mathbf{C}_u$ from the short period band would enable its removal from the entire band but $\mathbf{C}_d$ would still remain at longer periods. As the decomposition produces regional estimates which still contain up to 2 unknown static factors, there would be two shift level effects on the longest period impedance estimates.

Extension to Long Periods and Comparison with Undistorted Reference Impedance

At periods below a few cycles per day (cpd) an EM transfer function equivalent to the MT response $\mathbf{Z}_n$ can be obtained from purely magnetic data, using either the Sq or Dst source field (Schmucker, 1987). Although strong experimental efforts are necessary to obtain stable long period magnetotelluric data, the MT method can be extended to the same frequency range. A comparison of the MT tensor impedance and the scalar magnetic reference impedance then yields a complete distortion matrix at low frequencies (Junge, 1988). However, that distortion matrix is only useful as long as the 3D structure has a scale insufficient to produce strong anomalous magnetic fields at those periods. This case is described by Equation (7b). The relative level between apparant resistivities can be obtained from the MT tensor and one static shift factor is fixed by comparison to the reference impedance.

As an example, in Figure 13 MT and magnetic reference impedances of three sites in Germany are displayed for the frequency range 2–3 cpd. The magnetic reference impedances are close together, indicating no dramatic upper mantle conductivity anomalies in that target area. In contrast, the MT impedances vary strongly from site to site. This indicates the presence of anomalies which are small compared to the penetration depth at 2–3 cpd (400 km).

In terms of Equation (10), the low frequency reference technique yields the product tensor $\mathbf{C}_u \mathbf{C}_d$. This distortion matrix cannot simply be used to remove the static shifts at all higher frequencies. In particular, some crustal structures which affect the DC distortion matrix at low frequencies will act as an inductive anomaly at some high frequency.

A second constraint of this technique is that very strong conductivity anomalies, e.g. at a land-ocean transition create an anomalous magnetic field even at frequencies below a few cpd. The effect of these anomalous fields have to be removed

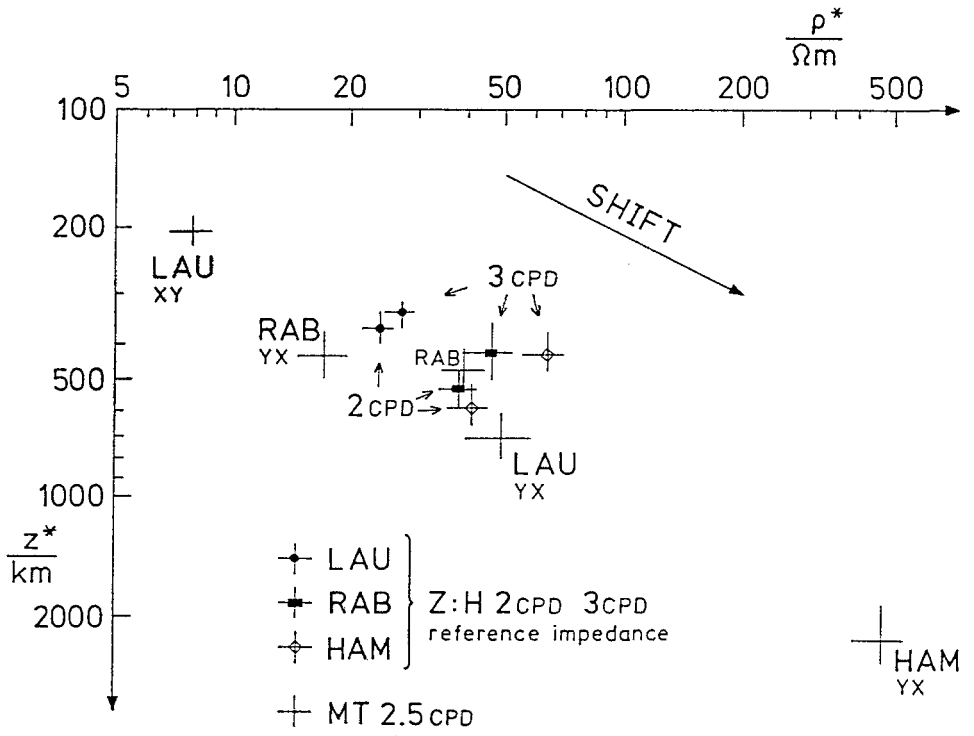

Fig. 13. Low frequency impedances of three sites in Central Europe plotted as modified apparent resistivities vs. penetration depth. Crosses labelled XY or YX refer to shifted magnetotelluric impedances. Other symbols refer to the magnetic reference impedance obtained for the 2nd and 3rd harmonic of the Sq source field.

from the flow frequency magnetic data prior to the calculation of the magnetic reference impedance (Bahr and Filloux, 1989).

Magnetovariational Link to Undistorted Reference Site

This method is a combination of the MT and the magnetovariational (MV) technique in the same frequency range (Jensen and Sierra, 1988). In the other two techniques mentioned, distortion matrices for very high or very low frequencies are calculated but this method is applied in the mid-frequency band (several seconds to several hours). In this frequency band, deep crustal conductivity anomalies may provide an inductive rather than a galvanic response. If the inductive anomaly is roughly 2D, then Equation (10) is replaced by

$$\mathbf{Z} = \mathbf{C}_u \mathbf{Z}_2 \tag{11}$$

where $\mathbf{C}_u$ refers to the galvanic response of a surface anomaly and $\mathbf{Z}_2$ refers to the inductive anomaly in the coordinate system of regional strike. Finding this regional strike then requires the decomposition that involves the most complicated

a priori model where, depending on the resolution problem referred to above, up to ten parameters occur. Two of them are found by use of the magnetovariational link to an undistorted reference site. In contrast, the "surface layer" and "reference impedance" techniques may be applied to field situations that involve less complex *a priori* models.

The inductive anomaly will, in turn, create inductive lateral changes of magnetic variations. These can be measured by use of magnetovariational transfer functions between different sites. Except for strong channelling, the MV transfer functions are not affected by the surface structures. The "magnetovariational link" method requires at least one site where no static shifts occur or where they have already been removed by use of some other method. Then, three sets of field data are interpreted with the same regional model: (I) The tensor impedance, free of local distortion, of the reference site; (II) the regional phases of the impedance at the distorted site; (III) magnetovariational transfer functions which link both sites. Figure 14 shows an example of the data sets (II) and (III) along with the corresponding model data. The model was used by Tezkan (1988) to obtain the static shift factors for some sites in the Black Forest, Germany. The magnetovariational link technique has also been described by Bahr (1988).

The site-to-site variations of the MV transfer functions are caused by lateral changes of conductance. In contrast, static shifts are related to a strong conductivity jump but only a minor conductance jump. The correct resistivity levels at the distorted site can then only be found if MV transfer functions over a wide frequency range are considered. The magnetovariational transfer functions (in particular, the induction vectors) should provide an independent check of the regional strike. However, in those cases where there is strong 3D galvanic scattering effects on the electric fields there will normally be generated an anomalous 3D magnetic field which will include a vertical component. The possible distortion of the induction vectors by this anomalous field must be taken into consideration.

Spatial Filtering or Spatial Averaging

Different techniques have been developed that incorporate multiple measurement of electric fields along a profile. The influence of local structures can be reduced by applying a spatial filter to the sequence of impedances along the profile (Torres-Verdin and Bostick, 1992; Jones *et al.*, 1989). Other authors argue against the application of a filter but rather the use of extremely long electrode separations to average out the influence of local structures (Groom and Bailey, 1989b). Figure 15 shows the field set-up and the resulting sounding curve of Brasse and Junge (1984) who used a gas pipeline in order to obtain long electrode separation.

Normally, the spatial filtering and spatial averaging technique provide no estimation of a distortion tensor but only a scalar distortion factor at each site. As a consequence, two constraints arise: (1) As long as only the telluric field in one

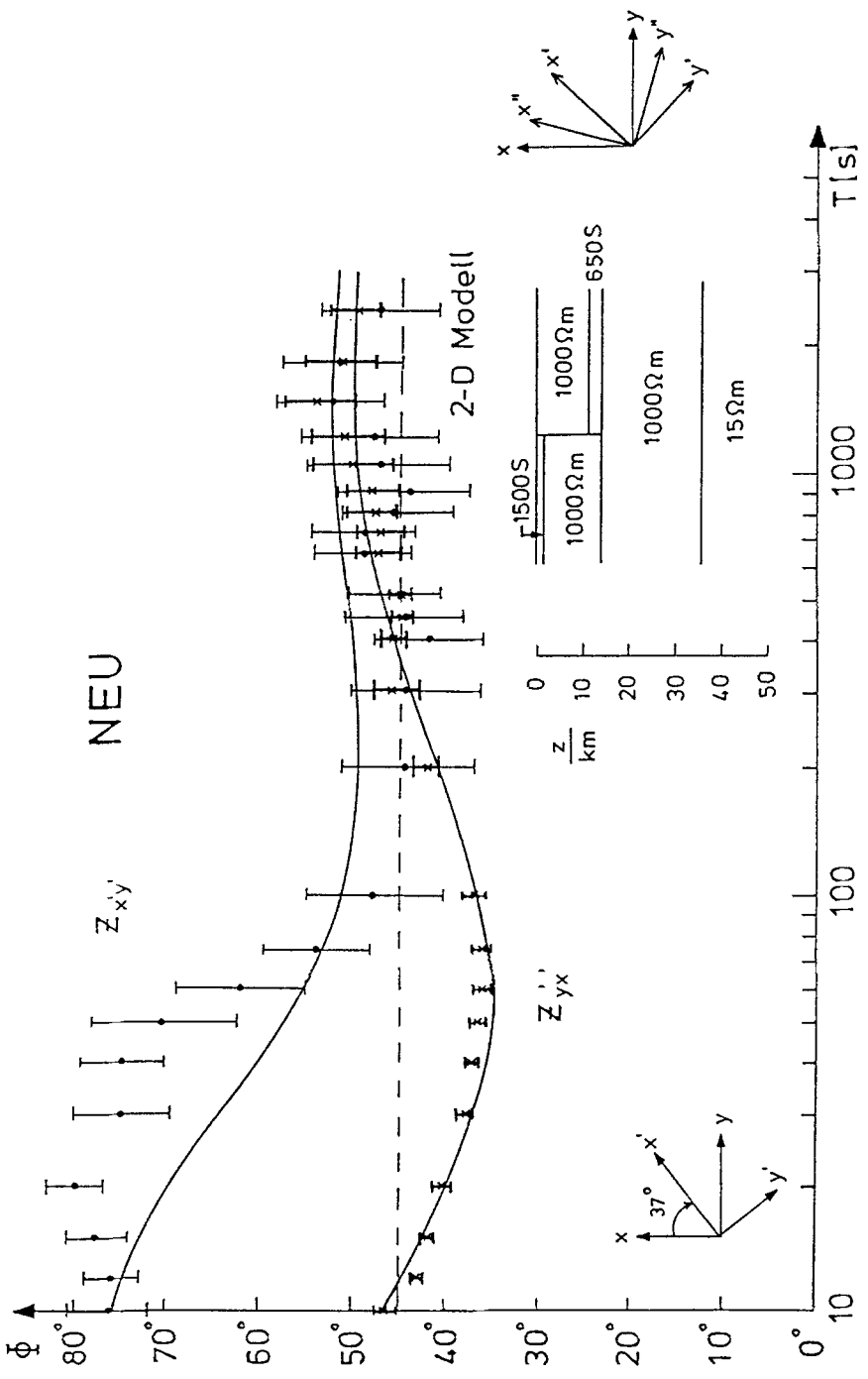
NEU
2-D Modell
$Z_{x'y'}$
$Z_{y'x'}$
Φ
80°
70°
60°
50°
40°
30°
20°
10°
0°
10
100
1000
T[s]
1500S
650S
1000Ωm
1000Ωm
1000Ωm
15Ωm
0
10
20
30
40
50
z/km
37°
x
x'
y
y'
x''
y''

(top)

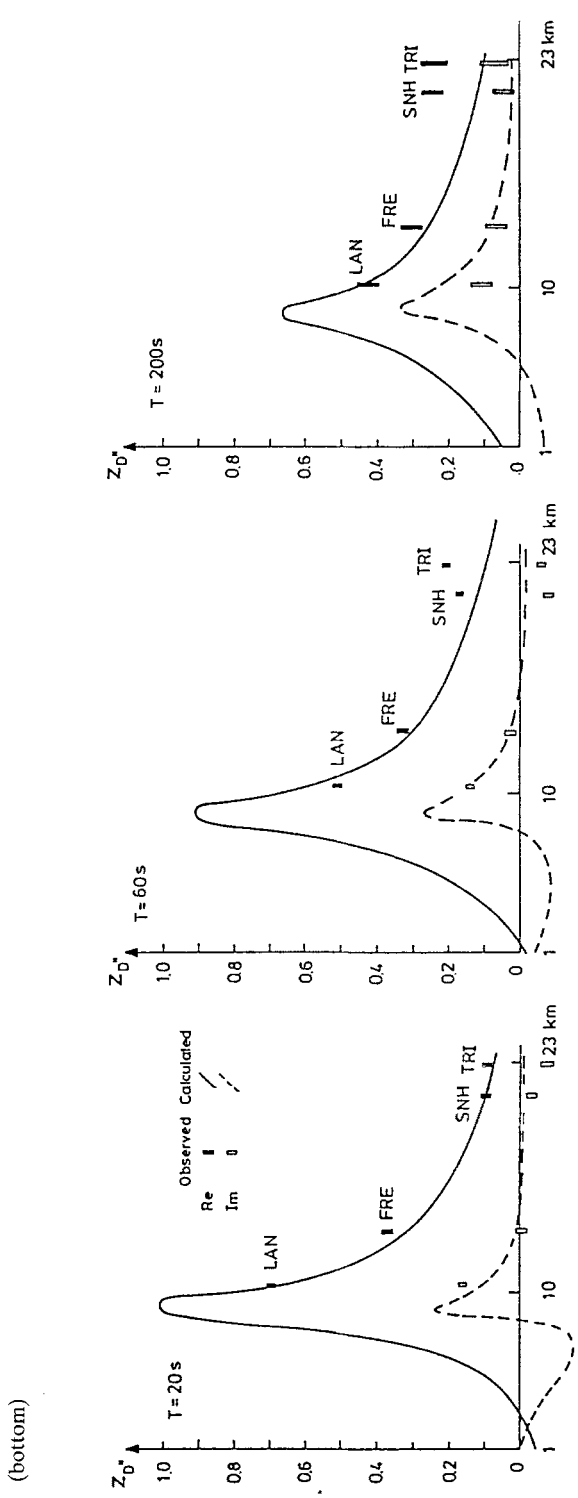

Fig. 14. Scaling correction of MT impedances of sites in the Black Forest, Germany, by use of the Magnetovariational link to an undistorted reference site (Tezkan, 1988). Top: The two regional phases of one site in the x', y' rotated co-ordinates. The regional 2D model is also plotted as vertical cut in y''-direction. Bottom: Magnetovariational transfer-function in y''-direction as a function of distance from the reference site.

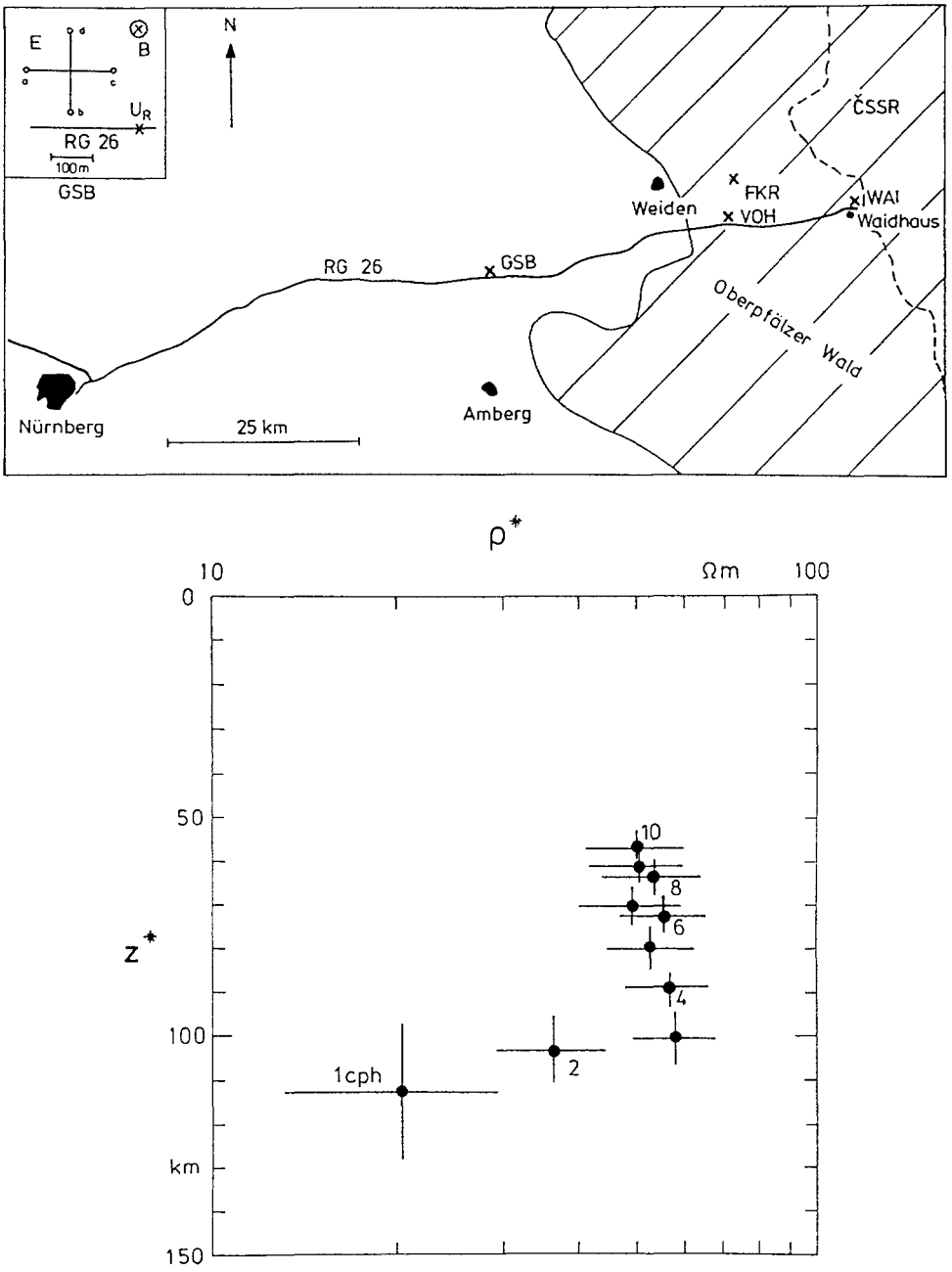

Fig. 15. Top: Gas pipeline used by Brasse and Junge (1984) for spatial averaging of the impedance. Bottom: the resulting sounding curve.

direction is considered, the resulting impedances may contain mixtures of two regional impedances. (2) This method may help correct the static shift levels in the decomposed apparent resistivities, but it is not clear how to correct any phase effects in the MT data due to 3D structures. The third constraint of this method has already been mentioned with respect to the mapping techniques: If the extension of the local structure is unknown, any filter length or electrode separation might be insufficient.

Examples with Field Data

The physically-based decompositions, in themselves, cannot remove all of the galvanic near-surface effects upon the impedance magnitudes as discussed above. However if the physical model for the decomposition is correct, then after processing the regional phase estimates should be close to the true regional phase responses. As such, they should vary smoothly from site to site and show a regional pattern. Decomposition analyses of a set of more than 32 MT sites, over more than 100 km of the Canadian Southern Cordillera (Jones *et al.*, 1988), has indicated an effective 2D strike over the entire region containing the sites. Although the phases for the 5 sites shown (Figure 10) cover a line of more than 35 km, decomposed responses indicate a well-resolved phase split for periods as long as 300 seconds. The phase-split implies that there is some sort of electrical anisotropy not only in the lower crust but also in the upper mantle.

For these data, the near-surface structure was particular to the individual site while the underlying background structure appears relatively uniform over large distances. In this case, the near-surface splitting or anisotropy after decomposition is assumed to be only due to the local structures which in fact determines which was termed $\mathbf{C}_u$. In many cases, the near surface structure was determined to be 3D over 1D with the 2D inductive structure strong only at periods greater that 1 second. In this case, the near surface impedances after the Groom and Bailey decomposition can simply be written as

$$gZ_0(\omega)\begin{pmatrix} 1+s & 0 \\ 0 & 1-s \end{pmatrix}\mathbf{I}, \tag{12}$$

where $\mathbf{I}$ is the identity matrix and $Z_0(\omega)$ is the 1D response at the higher frequencies. The anisotropy factor, s, can be determined and removed simply by arithmetic averaging so that only a single shift factor g remains in the estimated impedances. Analytic studies have indicated that this factor is only large if the site is on a near-outcropping scatterer.

Figure 16 compares responses after anisotropy correction for 5 sites which cover most of the survey line. The bottom left figure compares the corrected apparent resistivities for two westerly sites. The phase responses of these sites are plotted

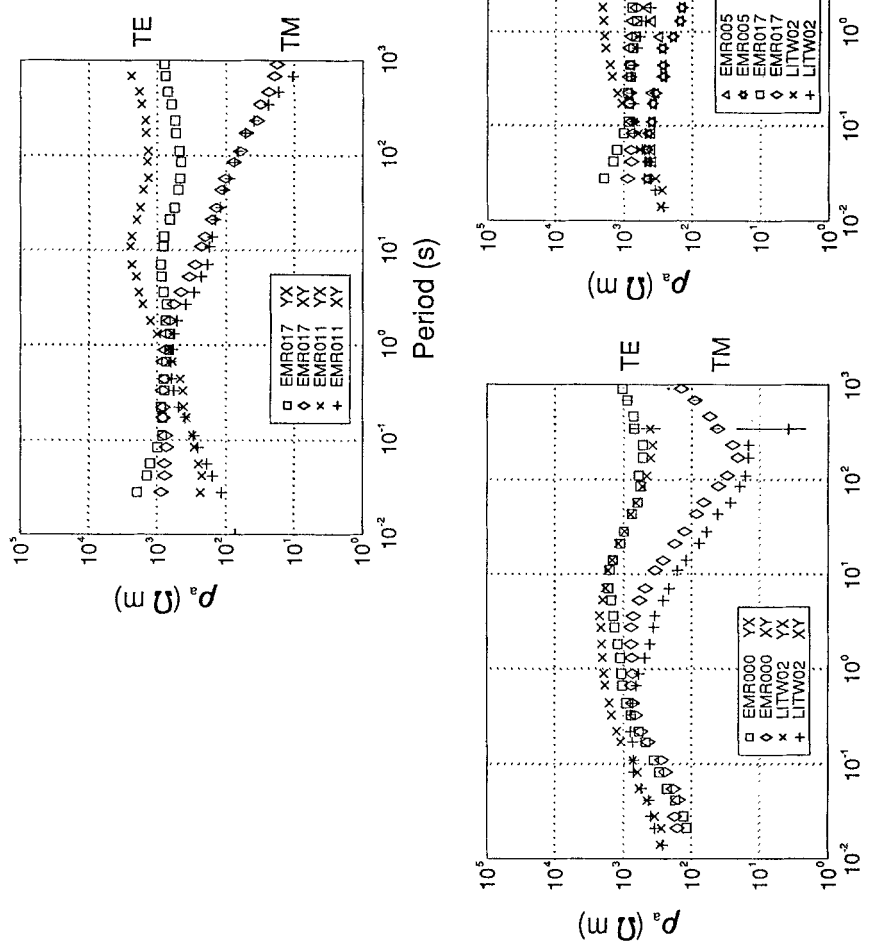

Fig. 16. Field example from the Canadian Southern Cordillera showing corrected regional impedance magnitude estimates after decomposition. Some corresponding phases are given in Figure 10. Left: Westerly sites, top: Easterly Sites, Right: Comparison of a westerly (LITW02), an easterly (EMR017) and a central site (EMR005).

in Figure 10. The bottom right figure contains comparisons of a westerly, a central and an easterly site while the top figure compares two easterly sites. Notice how in the left and right figures the TE apparent resistivities at long periods are not only parallel but have very near the same levels. The TM responses are parallel but at somewhat different levels. This would be expected in true 2D data. However, site EMR011 seemingly has its magnitudes still shifted up. It is possible that at this site the remaining scaling factor, g, is relatively large.

In the second example (Figure 17), phases from five sites in the vicinity of the German deep drilling project in east Bavaria are displayed. The sites are situated within a square of 5 km on a side. All five sites are influenced by strong local distortion. Figure 17 (top) show the phases after conventional 2D rotation. Figure 17 (bottom) shows the regional phases after decomposition. The conventional rotation yields very unstable phases because of the mixing effects referred to above. The decomposition yields two regional phases which indicate that a regional 2D structure can be recovered after removal of local distortion. The regional strike was found to be east-west coinciding with the strike indicated by the long period induction vectors (Bahr, 1991).

Conclusion

One, two and three-dimensional parametrizations of the magnetotelluric impedance tensor all have their place in a data interpretation scheme. However, three dimensional scattering effects can result in extremely incorrect structural interpretations if an incomplete analysis is done. Although the first-order effects of electric field scattering can be the most severe effect, magnetic effects caused either by the current channelling or induction can have significant effects on the estimated phases. Incorrect determination of the regional strike will reduce the phase separation between TE and TM modes and obviously lead to erroneous structural interpretation.

Although present three-dimensional decompositions can be extremely useful, they are also fraught with many problems. Strong current channelling can lead to a poorly determined inverse problem. Large noise coupled with a weak 2D inductive response results in a poorly resolved strike direction. 3D phase effects from an anomalous magnetic field adds to these problems. Nevertheless, correct analysis of the data with conventional, mathematical and galvanic 3D decomposition methods adds valuable information about the scattering processes governing the data.

A large problem remaining after 3D decomposition is correcting the levels of the recovered regional impedances. A number of methods are available for doing this although each has its own drawbacks and advantages. Multiple methods which are consistent with each other is probably the wisest choice at present. Additionally, care must be taken that 3D phase effects are not present in the recovered regional impedances prior to 2D inversion.

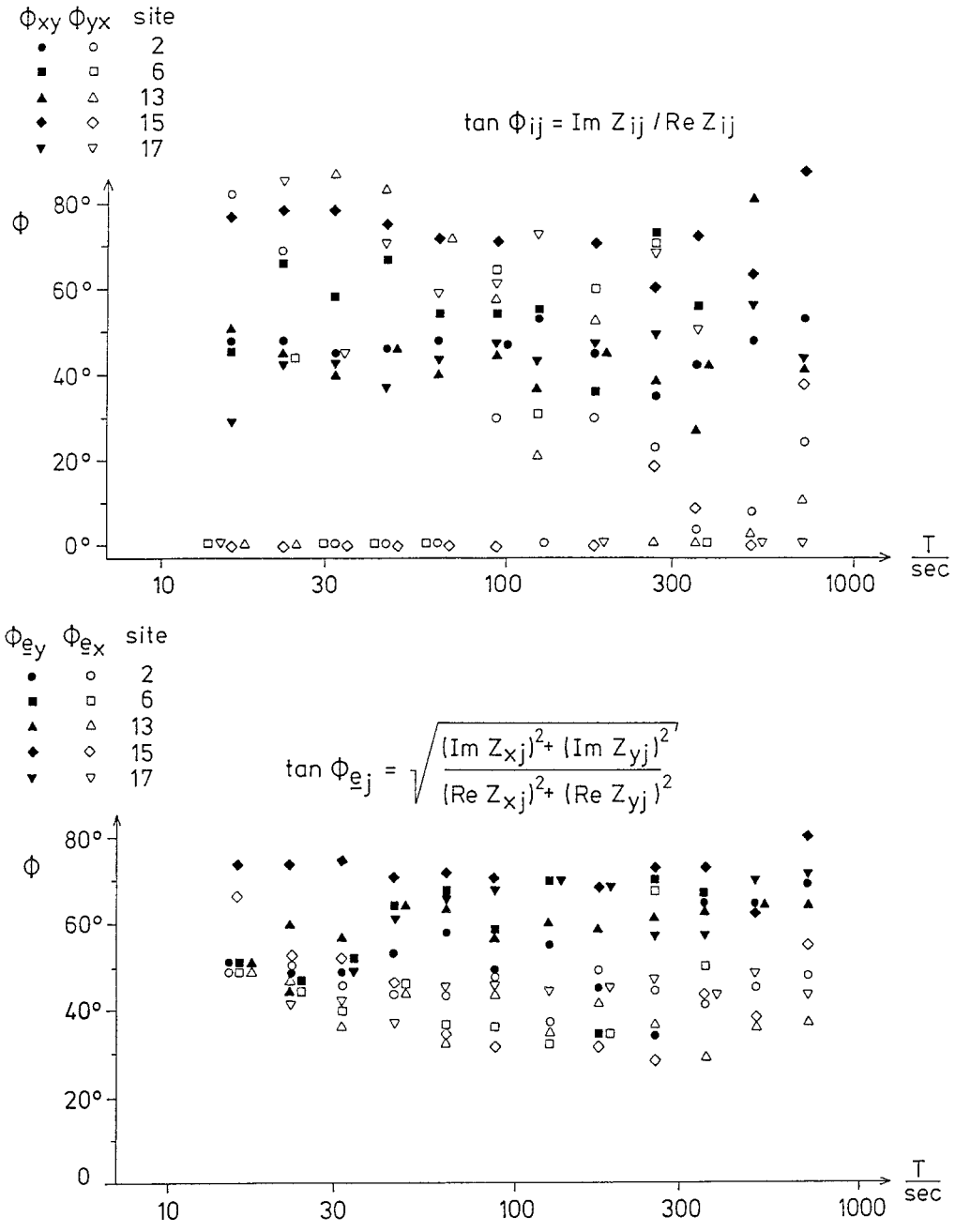

Fig. 17. Field Data example from the German deep drilling site. Top: Phases of the two principal impedances after rotation into the co-ordinate system of Swift's (1967) strike. Bottom: Phases of the two regional impedances.

Acknowledgements

The frame of this tutorial was compiled in San Diego the week prior to its presentation in Ensenada, Mexico at the 10th Electromagnetic Induction Workshop. We wish to thank George Jiracek and Linda Moeller for their extensive logistical help and generous hospitality during this time. Without their assistance this paper would not have been possible. We would also like to thank Drs. David Boerner, Toivo Korja and Alan Jones for reviewing the manuscript and Mr. Francois Richard for his assistance in preparing the figures. One of us (K.B.) acknowledges the financial support by the German Science Foundation under contract Ha 1210/7-1. Geological Survey of Canada Contribution #32591. Lithoprobe Publication # 267.

References

Tutorial

Bahr, K.: 1991, 'Geological Noise in Magnetotelluric Data: A Classification of Distortion Types', *Phys. Earth Planet. Int.* **60**, 24–38.

Cagniard, L.: 1953, 'Basic Theory of the Magneto-Telluric Method of Geophysical Prospecting', *Geophysics* **18**, 605–635.

Cerv, V. and Pek, J.: 1990, 'Modelling and Analysis of Electromagnetic Fields in 3D Inhomogenous Media', *Surveys in Geophysics* **11**, 205–229.

Hohmann, G. W.: 1976, 'Three-Dimensional Induced Polarization and Electromagnetic Modeling', *Geophysics* **40**, 309–324.

Groom, R. W. and Bailey, R. C.: 1991, 'Analytic Investigation of the Effects of Near-Surface 3D Galvanic Scatterers on MT Tensor Decompositions', *Geophysics* **56**, 496–518.

Habashy, T. M., Groom, R. W. and Spies, B.: 1991, 'Low-Frequency 3D EM Scattering Effects in Conducting Media, Limitations on the Born Approximation, and an Extended Born Approximation', Progress in Electromagnetics Research Symposium, July 1991.

Jones, A. G.: 1983, 'The Problem of Current Channeling: A Critical Review', *Geophysical Surveys* **6**, 79–122.

Jiracek, G.: 1990, 'Near Surface and Topographic Distortions in Electromagnetic Induction', *Surveys in Geophysics* **11**, 163–203.

West, G. F. and Edwards, R. N.: 1985, 'A Simple Parametric Model for the Electromagnetic Response of an Anomalous Body in a Host Medium', *Geophysics* **50**, 2542–2559.

Structural dimensionality

Groom, R. W., Kurtz, R. D., Jones, A. G. and Boerner, D. E.: 1991, 'A Quantitative MT Methodology for Determining the Dimensionality of Structure', submitted *Geophysical Journal International.*

Jones, A. G., Kurtz, R. D., Oldenburg, D. W., Boerner, D. E. and Ellis, R.: 1988, 'Magnetotelluric Observations Along the Lithoprobe Southeastern Canadian Cordilleran Transect', *Geophysical Research Letters* **15**, 677–680.

Ranganayaki, R. P.: 1984, 'An Interpretive Analysis of Magnetotelluric Data', *Geophysics* **49**, 1730–1748.

Swift, C. M.: 1967, 'A Magnetotelluric Investigation of an Electrical Conductivity Anomaly in the South Western United States', Ph.D. thesis, M.I.T., Cambridge, Mass.

Mathematical decompositions

Eggers, D. W.: 1982, 'An Eigenstate Formulation of the Magnetotelluric Impedance Tensor', *Geophysics* **47**, 1204–1214.

LaToracca, G. A., Madden, T. R. and Korringa, J.: 1986, 'An Analysis of the Magnetotelluric Impedance Tensor for Three-Dimensional Structures', *Geophysics* **51**, 1819–1829.

Spitz, S.: 1985, 'The Magnetotelluric Impedance Tensor Properties with Respect to Rotations', *Geophysics* **50**, 1610–1617.

Yee, E. and Paulson, K. V.: 1987, 'The Canonical Decomposition and its Relationship to Other Forms of Magnetotelluric Impedance Tensor Analysis', *J. Geophys.* **61**, 173–189.

Physical decompositions

Bahr, K.: 1988, 'Interpretation of the Magnetotelluric Impedance Tensor: Regional Induction and Local Telluric Distortion', *J. Geophys.* **62**, 119–127.

Groom, R. W. and Bailey, R. C.: 1989a, 'Decomposition of the Magnetotelluric Impedance Tensor in the Presence of Local Three-Dimensional Galvanic Distortion', *J. Geophys. Res.* **94**(B2), 1913–1925.

Modelling c by the use of additional information about the surface layer

Berdichevsky, M. N. and Dmitriev, V. I.: 1976, 'Distortion of Magnetic and Electric Fields by Near-Surface Lateral Inhomogeneities', *Acta Geodaet., Geophys. et Montanist. Acad. Sci. Hung.* **11**, 447–483.

Craven, J. A., Jones, A. G., Boerner, D. E., Groom, R. W. and Kurtz, R. D.: 1990, 'The Correction of Static Shift in Magnetotelluric Data from the Lithoprobe Southern Canadian Cordillera Transect', *60th Annual Intl. Mtg., Soc. Expl. Geophys.*, Expanded Abstracts, pp. 561–564.

Kemmerle, K.: 1977, 'Magnetotellurik am Alpen-Nordrand mit Diskussion der lokalen Effekte und einer Einzeleffekt-Auswertung', Diss. Fachb. Geowissenschaften, München.

Pellerin, L. and Hohmann, J. W.: 1990, 'Transient Electromagnetic Inversion: A Remedy for Magnetotelluric Static Shifts', *Geophysics* **55**, 1242–1250.

Spies, B. R.: 1989, 'Depth of Investigation of Electromagnetic Sounding Methods', *Geophysics* **54**, 872–888.

Sternberg, B. K., Washburne, J. C. and Pellerin, L.: 1988, 'Correction for the Static Shift in Magnetotellurics Using Transient Electromagnetic Soundings', *Geophysics* **53**, 1459–1468.

Extension to long periods and comparison with undistorted reference impedance

Bahr, K. and Filloux, J. H.: 1989, 'Local Sq Response Functions from EMSLAB Data', *J. Geophys. Res.* **94**(B10), 14195–14200.

Junge, A.: 1988, 'The Telluric Field in Northern Germany Induced by Tidal Motion in the North Sea', *Geophys. J.* **95**, 523–533.

Larsen, J. C.: 1977, 'Removal of Local Surface Conductivity Effects from Low Frequency Mantle Response Curves', *Acta Geodaet., Geophys. et Montanist. Acad. Sci. Hung.* **12**, 183–186.

Schmucker, U.: 1987, 'Magnetic and Electric Fields Due to Electromagnetic Induction by External Sources', in K. Fuchs and H. Soffel (eds.), *Landolt–Brnstein, Numerical Data and Function Relationships in Science and Technology, New ser., Group V: Geophys. Space Res., subvol IIb*, Springer, New York, pp. 100–124.

MAGNETOVARIATIONAL LINK TO UNDISTORTED REFERENCE SITE

Bahr, K.: 1988, 'Interpretation of the Magnetotelluric Impedance Tensor: Regional Induction and Local Telluric Distortion', *J. Geophys.* **62**, 119–127.

Jensen, V. and Sierra, J. L.: 1988, 'Case History: The ECRE Method Applied to a Two Dimensional Salt Structure', Geometra Ltd. Publication, 16 pp.

Tezkan, B.: 1988, 'Electromagnetic Sounding Experiments in the Schwarzwald Central Gneiss Massif', *J. Geophys.* **62**, 109–118.

SPATIAL FILTERING OR SPATIAL AVERAGING

Groom, R. W. and Bailey, R. C.: 1989b, 'Some Effects of Multiple Lateral Inhomogeneities in Magnetotellurics', *Geophysical Prospecting* **37**, 697–712.

Jones, A. G., Boerner, D. E., Kurtz, R. D., Oldenburg, D. W. and Ellis, R.: 1989, 'EMAP Data Processing in the Wavenumber Domain', *59th Annual Intl. Mtg., Soc. Expl. Geophys.*, Expanded Abstracts, p. 172.

Torres-Verdin, C. and Bostick, F. X.: 1992, 'Principles of Spatial Surficial Electric Field Filtering in Magnetotellurics: Electromagnetic Array Profiling (EMAP)', accepted for *Geophysics*.

Brasse, H. and Junge, A.: 1984, 'The Influence of Geomagnetic Variations on Pipelines and an Application for Large-Scale Magnetotelluric Depth Sounding', *J. Geophys.* **55**, 31–36.